Cell Metabolism

Article

Non-canonical Glutamate-Cysteine Ligase Activity Protects against Ferroptosis

Graphical Abstract

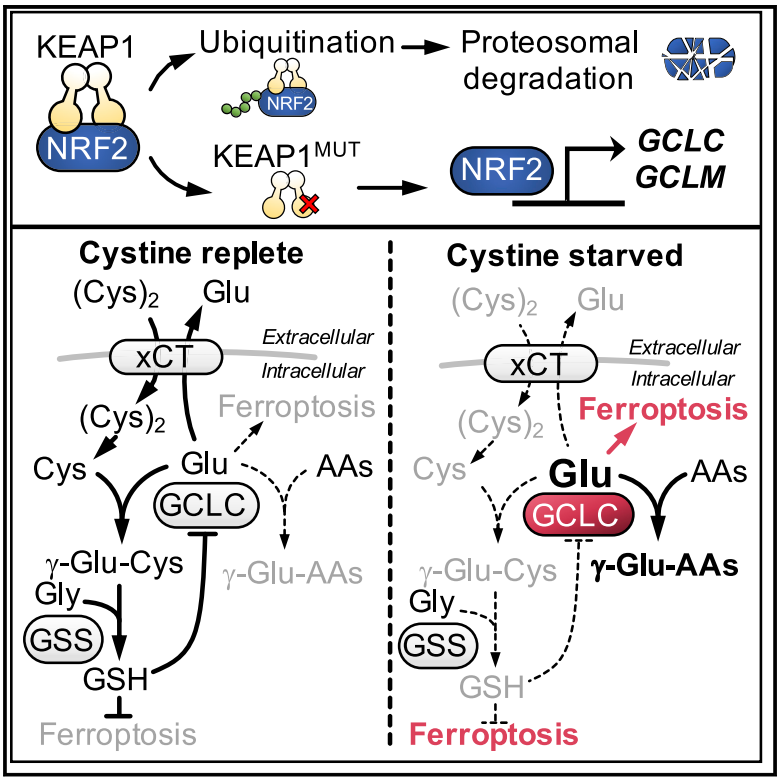

Highlights

- Cystine starvation induces γ-glutamyl-peptide accumulation in NSCLC cells
- GCLC catalyzes γ-glutamyl-peptide synthesis via a GSH-independent mechanism
- NRF2 protects against ferroptosis via γ-glutamyl-peptide synthesis
- γ-glutamyl-peptide synthesis prevents ferroptosis by reducing glutamate stress

Authors

Yun Pyo Kang, Andrea Mockabee-Macias, Chang Jiang, ..., Everett Stone, Isaac S. Harris, Gina M. DeNicola

Correspondence

gina.denicola@moffitt.org

In Brief

GCLC catalyzes the first step in glutathione synthesis via the ligation of cysteine with glutamate. Kang et al. demonstrate that under cysteine-limiting conditions, GCLC instead ligates glutamate with alternative amino acids, thereby scavenging glutamate to protect against ferroptosis.

Kang et al., 2021, Cell Metabolism *33*, 1–16
January 5, 2021
https://doi.org/10.1016/j.cmet.2020.12.007

CellPress

Please cite this article in press as: Kang et al., Non-canonical Glutamate-Cysteine Ligase Activity Protects against Ferroptosis, Cell Metabolism (2020), https://doi.org/10.1016/j.cmet.2020.12.007

Cell Metabolism

CellPress

Article

Non-canonical Glutamate-Cysteine Ligase Activity Protects against Ferroptosis

Yun Pyo Kang,[1] Andrea Mockabee-Macias,[1] Chang Jiang,[1] Aimee Falzone,[1] Nicolas Prieto-Farigua,[1] Everett Stone,[2] Isaac S. Harris,[3] and Gina M. DeNicola[1,4,*]

[1]Department of Cancer Physiology, H. Lee. Moffitt Cancer Center, Tampa, FL 33612, USA
[2]Department of Molecular Biosciences, University of Texas at Austin, Austin, TX 78712, USA
[3]University of Rochester Medical Center, Rochester, NY 14642, USA
[4]Lead Contact
*Correspondence: gina.denicola@moffitt.org
https://doi.org/10.1016/j.cmet.2020.12.007

SUMMARY

Cysteine is required for maintaining cellular redox homeostasis in both normal and transformed cells. Deprivation of cysteine induces the iron-dependent form of cell death known as ferroptosis; however, the metabolic consequences of cysteine starvation beyond impairment of glutathione synthesis are poorly characterized. Here, we find that cystine starvation of non-small-cell lung cancer cell lines induces an unexpected accumulation of γ-glutamyl-peptides, which are produced due to a non-canonical activity of glutamate-cysteine ligase catalytic subunit (GCLC). This activity is enriched in cell lines with high levels of NRF2, a key transcriptional regulator of GCLC, but is also inducible in healthy murine tissues following cysteine limitation. γ-glutamyl-peptide synthesis limits the accumulation of glutamate, thereby protecting against ferroptosis. These results indicate that GCLC has a glutathione-independent, non-canonical role in the protection against ferroptosis by maintaining glutamate homeostasis under cystine starvation.

INTRODUCTION

Amino acids can play critical biosynthetic functions beyond their use for protein synthesis. A notable example is the thiol-containing amino acid cysteine. Cysteine-derived molecules are crucial for multiple cellular processes as a consequence of their sulfur moiety, which facilitates diverse functions, including enzyme catalysis, energy transfer, and redox metabolism (Furuyama and Sassa, 2000; Martínez-Reyes et al., 2016; Rouault, 2012; Solmonson and DeBerardinis, 2018; Vyas et al., 2016). Cysteine is a rate-limiting substrate for the synthesis of glutathione (GSH) (Stipanuk et al., 2006), the most abundant intracellular antioxidant (Winterbourn and Hampton, 2008). GSH is a tripeptide consisting of the amino acids cysteine, glutamate, and glycine. The synthesis of GSH occurs in two steps (Anderson, 1998). First, glutamate and cysteine are ligated by GCLC, producing the dipeptide γ-glutamyl-cysteine (γ-Glu-Cys). Next, glycine is added to γ-Glu-Cys, producing the tripeptide GSH (γ-Glu-Cys-Gly). The antioxidant activity of GSH is a consequence of its function as a cofactor to multiple antioxidant proteins, including glutaredoxins (GRXs), GSH peroxidases (GPXs), and GSH S-transferases, thereby removing reactive oxygen species (ROS) (Harris and DeNicola, 2020).

Because of both its reactive thiol moiety and its essential function in redox homeostasis, cysteine levels are tightly regulated. While cysteine excess is prevented by overflow into the taurine pathway (Stipanuk et al., 2009), cysteine demand is met by inducible regulation of cystine import. Following oxidative stress, the expression of the cystine/glutamate exchange transporter xCT is induced (Habib et al., 2015), thereby facilitating the uptake of cystine and its reduction to cysteine. In some tissues, most notably the liver, cysteine is also synthesized from homocysteine and serine via the transsulfuration pathway (Beatty and Reed, 1980; Rao et al., 1990; Reed and Orrenius, 1977). Given the important roles of cysteine, many cancers overexpress xCT (Ji et al., 2018; Takeuchi et al., 2013; Timmerman et al., 2013), which is positively regulated by oncogenic RAS (Lim et al., 2019) and NRF2 (Sasaki et al., 2002), and negatively regulated by the tumor suppressor p53 (Jiang et al., 2015). Pharmacological targeting of cystine uptake can effectively induce cancer cell death (Cramer et al., 2017; Dixon et al., 2012; Zhang et al., 2019), and cystine starvation can impair growth in multiple *in vivo* cancer models (Cramer et al., 2017; Zhang et al., 2019).

Cysteine inadequacy can induce an iron-dependent form of cell death known as ferroptosis (Dixon et al., 2012). Ferroptosis is triggered by the reaction of polyunsaturated fatty acids (PUFAs) in membrane lipids with peroxyl radicals produced from iron (Fe^{2+}) and ROS (Cao and Dixon, 2016; Yang et al., 2014), thereby inducing lipid peroxidation. Consistently, processes that promote ferroptosis include increased ferritin uptake (Gao et al., 2015), ferritin degradation (Mancias et al., 2014), synthesis of PUFA-containing lipids (Dixon et al., 2015; Doll et al., 2017), polyamine synthesis-derived ROS (Zhang et al., 2020), and ROS production via other mechanisms (Gao et al., 2015,

Please cite this article in press as: Kang et al., Non-canonical Glutamate-Cysteine Ligase Activity Protects against Ferroptosis, Cell Metabolism (2020), https://doi.org/10.1016/j.cmet.2020.12.007

2019). Ferroptosis protection is conferred by parallel pathways that protect cells against membrane lipid peroxidation in GSH-dependent (Yang et al., 2014) and GSH-independent (Bersuker et al., 2019; Doll et al., 2019; Soula et al., 2020) manners. However, while cysteine is directly linked to GSH synthesis, which can influence both the levels of ROS and the activity of the lipid peroxidase GPX4, cysteine availability can also influence the levels of cofactors and metabolites associated with ferroptosis beyond its use for GSH synthesis, including the production of coenzyme A (Badgley et al., 2020; Leu et al., 2019) and iron-sulfur clusters (Alvarez et al., 2017). Importantly, the metabolic consequences of cystine starvation are poorly understood.

To understand the metabolic consequences of cystine starvation, we analyzed cysteine metabolism and cystine starvation-induced metabolic changes in non-small-cell lung cancer (NSCLC) cells, which we previously found are sensitive to cystine starvation (Kang et al., 2019). Surprisingly, we found that under cysteine-deprived conditions, GCLC substituted other small, non-charged amino acids for cysteine in the ligation with glutamate to generate γ-glutamyl-peptides. γ-glutamyl-peptide synthesis by GCLC was also evident in mouse tissues. This promiscuous activity prevented glutamate accumulation to protect against ferroptosis.

RESULTS

Transsulfuration Cannot Support NSCLC Cysteine Pools

To evaluate the consequence of cystine starvation in NSCLC cells, we starved a panel of cell lines of extracellular cystine and first monitored viability using fluorescent dyes that stain the nuclei of dead cells (Figure S1A), which were monitored over time using the Incucyte system. Cumulative cell death was calculated from the area under the curve (AUC), thereby facilitating comparisons between cell lines or treatments as previously described by others (Bersuker et al., 2019; Cao et al., 2019). Consistent with prior reports in lung and other cancer cell types (Badgley et al., 2020; Poursaitidis et al., 2017; Zhang et al., 2020), NSCLC cell death in response to cystine starvation exhibited features of the iron-dependent form of cell death known as ferroptosis. First, dead cells exhibited morphological features consistent with ferroptosis, rather than apoptosis, which could be rescued by both the lipid ROS scavenger and ferroptosis inhibitor Ferrostatin-1 (Fer-1) and the iron chelator deferoxamine (DFO) (Dixon et al., 2012) (Figure S1B). Moreover, lipid peroxide accumulation was observed prior to the onset of cell death, which was rescued by Fer-1 treatment (Figure S1C). Response of the NSCLC cell line panel to cystine starvation was heterogeneous, from the complete resistance of cell death out to 72 h to the immediate onset of cell death within hours, which was lipid peroxide- and iron-dependent in all lines assayed (Figures 1A and S1D).

NSCLC cell lines have a diverse spectrum of mutations associated with diverse metabolic phenotypes and metabolic requirements (Chen et al., 2019; DeNicola et al., 2015). To examine whether the heterogeneous onset of ferroptosis under cystine starvation was associated with maintenance of the cysteine pool via the transsulfuration pathway, which synthesizes cysteine *de novo* from methionine-derived homocysteine and serine, we performed a quantitative analysis of $^{13}C_3$-serine tracing into both cysteine and GSH. Cysteine is a rate-limiting metabolite of GSH synthesis (Stipanuk et al., 2006) and GSH also plays an important role in ferroptosis via ROS metabolism (Dixon et al., 2012) and as a substrate of GPX4 (Conrad and Friedmann Angeli, 2015). $^{13}C_3$-serine is metabolized to $^{13}C_2$-glycine (M+2) and $^{13}C_3$-cysteine (M+3), which are subsequently incorporated into GSH (M+2 and M+3, respectively; Figure 1B). Cells were labeled under cystine-replete and starved conditions for 4 h, which was sufficient to label most of the serine fraction and half of the glycine fraction irrespective of the presence of cystine (Figures 1C and 1D). In contrast, minimal to no M+3 labeling of cysteine was detected under both fed and starved conditions, demonstrating little to no transsulfuration capacity (Figure 1E). Consequently, cystine starvation for 4 h resulted in robust depletion of intracellular cysteine (Figure 1E). Moreover, both the amount of M+2 glycine incorporated into GSH and total GSH levels were lower across all cell lines following starvation (Figure 1F), demonstrating that GSH synthesis was impaired. These results indicate that *de novo* cysteine synthesis via transsulfuration cannot support intracellular cysteine levels in NSCLC cell lines, leading to impaired GSH synthesis as a consequence of cysteine depletion under cystine-starved conditions.

Cystine Starvation Induces Glutamate-Derived γ-Glutamyl-Peptide Accumulation

Despite a uniform depletion in intracellular cysteine, NSCLC cell lines had a heterogeneous induction of ferroptosis following cystine starvation. To identify additional cellular responses to starvation, we conducted non-targeted metabolomics in A549 cells. While most metabolites were depleted, we discovered an interesting cluster of unknown metabolites that were highly accumulated in cystine-starved cells (Figure 2A). Using authentic standards, these unknown metabolites were identified as γ-glutamyl-di- or tripeptides, which all contain a glutamate moiety (Figure 2A). Authentic standards for γ-glutamyl-threonine (γ-Glu-Thr) and γ-glutamyl-alanyl-glycine (γ-Glu-Ala-Gly) were not available, and thus we further validated their identity via stable isotope metabolite tracing. $^{13}C_5$, $^{15}N_2$-glutamine tracing validated that both γ-Glu-Thr and γ-Glu-Ala-Gly were derived from glutamate (Figures 2B and 2C), and 2, 3, 3-$^{2}H_3$-serine tracing validated that γ-Glu-Ala-Gly was derived from glycine (Figure S2A). Moreover, we found that the xCT inhibitor erastin, which could deplete intracellular cysteine in a manner similar to cystine starvation (Figure S2B), also induced the accumulation of γ-glutamyl-di- or tripeptides to similar levels in A549 cells (Figure S2C). In addition, although γ-glutamyl-dipeptides are typically thought to be derived from GSH by γ-glutamyl transferase (GGT) via the transfer of the GSH γ-glutamyl group to recipient amino acids extracellularly (Hanigan and Pitot, 1985), $^{13}C_5$, $^{15}N_2$-glutamine tracing demonstrated that while the newly labeled GSH fraction was very small, as expected, glutamate and γ-glutamyl-peptides were approximately 50% labeled in cystine-starved A549 cells (Figures 2B and 2C), suggesting that the γ-glutamyl-peptides were derived from glutamate, but not from GSH. Finally, the levels of γ-glutamyl-peptides were inversely correlated with cystine starvation-induced ferroptosis sensitivity across the panel of NSCLC cell lines (Figure 2D). These results demonstrate that cystine starvation promotes the accumulation

Please cite this article in press as: Kang et al., Non-canonical Glutamate-Cysteine Ligase Activity Protects against Ferroptosis, Cell Metabolism (2020), https://doi.org/10.1016/j.cmet.2020.12.007

CellPress

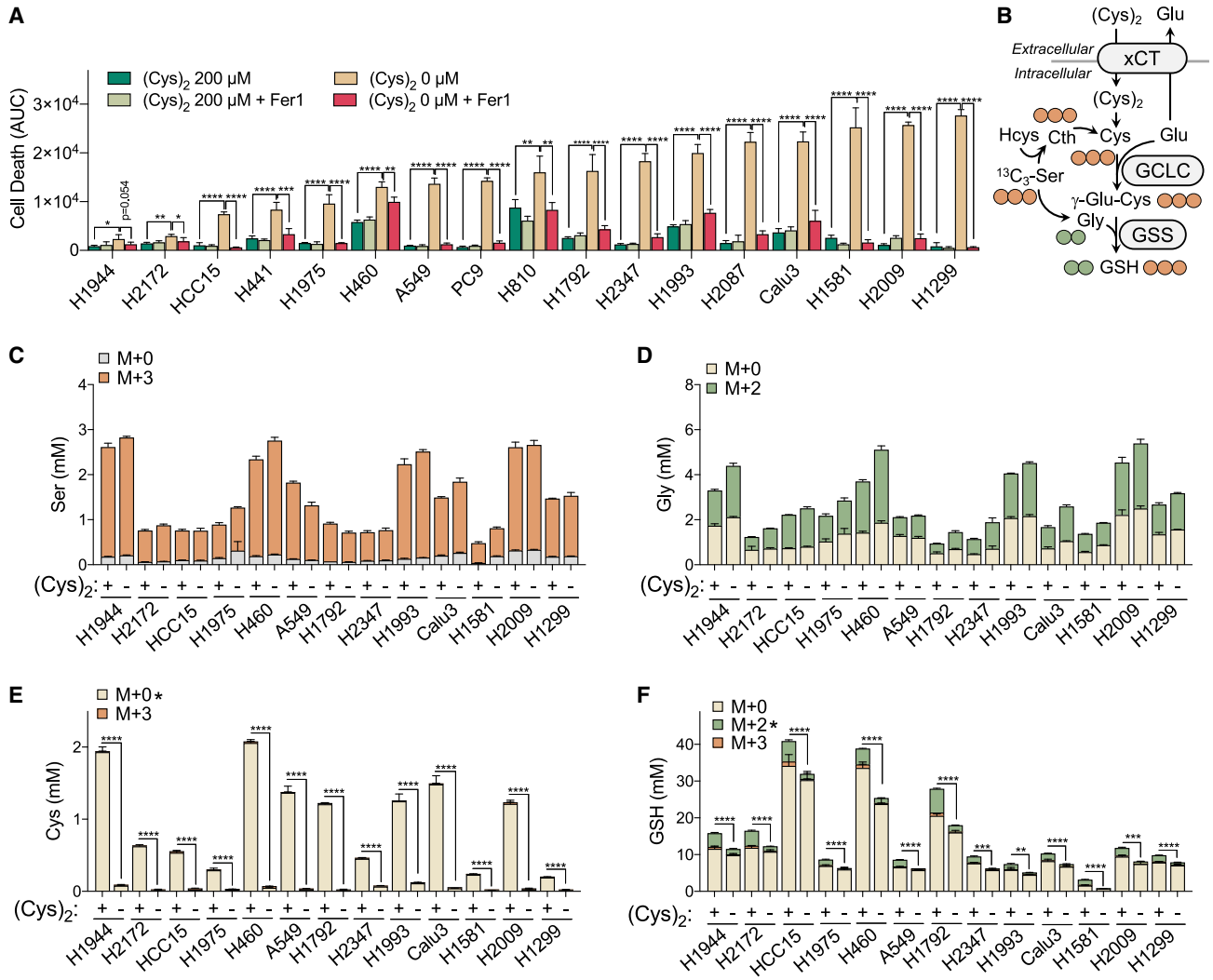

Figure 1. Transsulfuration Cannot Support NSCLC Cysteine Pools

(A) Measurement of NSCLC cell death under cystine-starved (0 μM) or -replete (200 μM) conditions treated with vehicle (0.1% DMSO) or Ferrostatin-1 (Fer-1, 10 μM) (N = 4). Cell death was determined by Incucyte analysis of Sytox Green staining over 73 h, followed by normalization to cell density. Area under the curve (AUC) calculations are presented here. Full curves can be found in Figure S1D.

(B) Schematic depiction of [$^{13}C_3$]-serine tracing into cysteine (M+3, 3 carbons labeled) and glutathione (M+2, 2 carbons labeled from glycine; M+3, 3 carbons labeled from cysteine).

(C–F) Quantitation of [$^{13}C_3$]-serine tracing into (C) serine, (D) glycine, (E) cysteine, and (F) glutathione (GSH) following culture under cystine-starved (–) or -replete (+) conditions for 4 h (N = 3).

For (A) and (C)–(F), data are shown as mean ± SD. N is number of biological replicates. *p < 0.05, **p < 0.01, ***p < 0.001, and ****p < 0.0001. For (A), a one-way ANOVA with Bonferroni's multiple comparison test was used for statistical analyses. An unpaired two-tailed t test was used for the statistical comparisons between non-labeled M+0 fraction in (E) and M+2 labeling fractions in (F).

of glutamate-derived γ-glutamyl-peptides, which may play a role in the cellular response to cystine starvation.

GCLC Mediates γ-Glutamyl-Peptide Synthesis

We next wanted to understand how cells were producing γ-glutamyl-peptides. Among our accumulated γ-glutamyl-peptides was the GSH-similar tripeptide γ-glutamyl-2-aminobutyryl-glycine (γ-Glu-2AB-Gly), also known as ophthalmic acid, which is synthesized by GCLC and GSS under cysteine-limiting conditions. In this process, 2-aminobutyrate is substituted for cysteine (Huang et al., 1988; Oppenheimer et al., 1979), suggesting GCLC may directly synthesize γ-glutamyl-peptides. Moreover, γ-glutamyl-valine is synthesized by the *Saccharomyces cerevisiae* glutamate-cysteine ligase (Sofyanovich et al., 2019), and γ-glutamyl-dipeptide synthesis by mouse liver extracts was recently shown to be GCLC-dependent (Kobayashi et al., 2020). Thus, we hypothesized that the γ-glutamyl-dipeptides were directly generated by GCLC rather than by GGT. Consistent with this hypothesis, we observed a strong correlation between the levels of γ-glutamyl-dipeptides with GCLC expression under cysteine-starved, but not cysteine-replete conditions across the NSCLC cell lines (Figure 3A).

Please cite this article in press as: Kang et al., Non-canonical Glutamate-Cysteine Ligase Activity Protects against Ferroptosis, Cell Metabolism (2020), https://doi.org/10.1016/j.cmet.2020.12.007

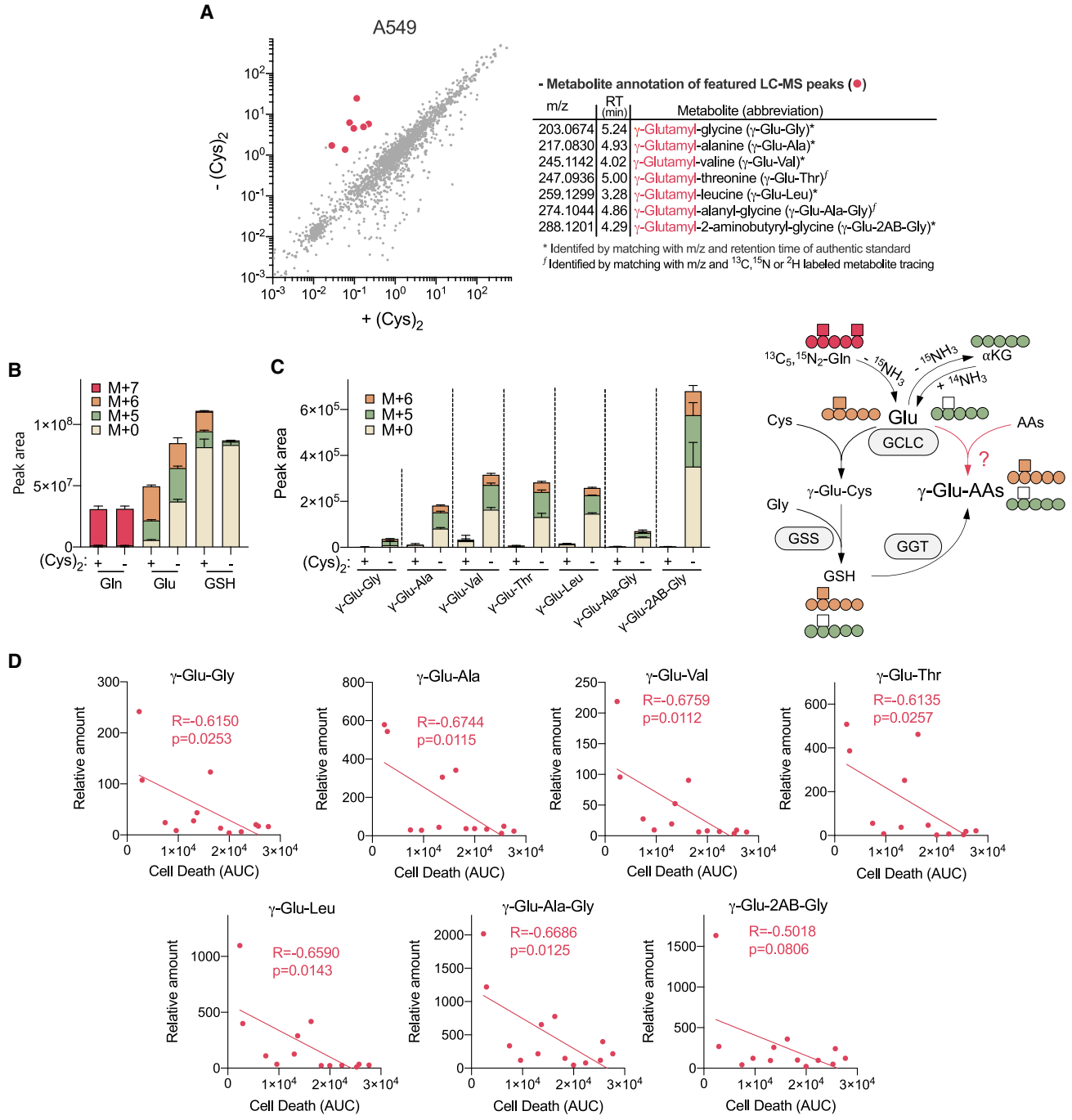

Figure 2. Cystine Starvation Induces Glutamate-Derived γ-Glutamyl-Peptide Accumulation

(A) Scatterplot comparison of non-targeted metabolomics features in A549 cells cultured under cystine-replete (+Cys_2) and -starved conditions (−Cys_2) for 4 h (left). The mean intensity of median-normalized LC-MS peaks of each group (N = 3) is plotted on the axes, and each dot represents an individual LC-MS peak. The LC-MS peaks that highly accumulated under cystine starvation (red dots) were further identified and annotated (right).

(B and C) A549 cell $^{13}C_5$, $^{15}N_2$-Gln tracing into (B) Gln, Glu, GSH, and (C) γ-Glu-peptides following culture in cystine-replete or -starved conditions for 4 h (N = 3).

(D) Correlation between ferroptotic cell death (AUC, from Figure 1A) and the levels of γ-Glu-peptides across 13 NSCLC cell lines. The γ-Glu-peptides were analyzed following cystine starvation for 12 h and normalized to the mean value of H1581 cells under cystine-replete conditions (N = 13).

For (B) and (C), data are shown as mean ± SD. N is number of biological replicates. For (D), Pearson correlation test was used for statistical analysis.

Please cite this article in press as: Kang et al., Non-canonical Glutamate-Cysteine Ligase Activity Protects against Ferroptosis, Cell Metabolism (2020), https://doi.org/10.1016/j.cmet.2020.12.007

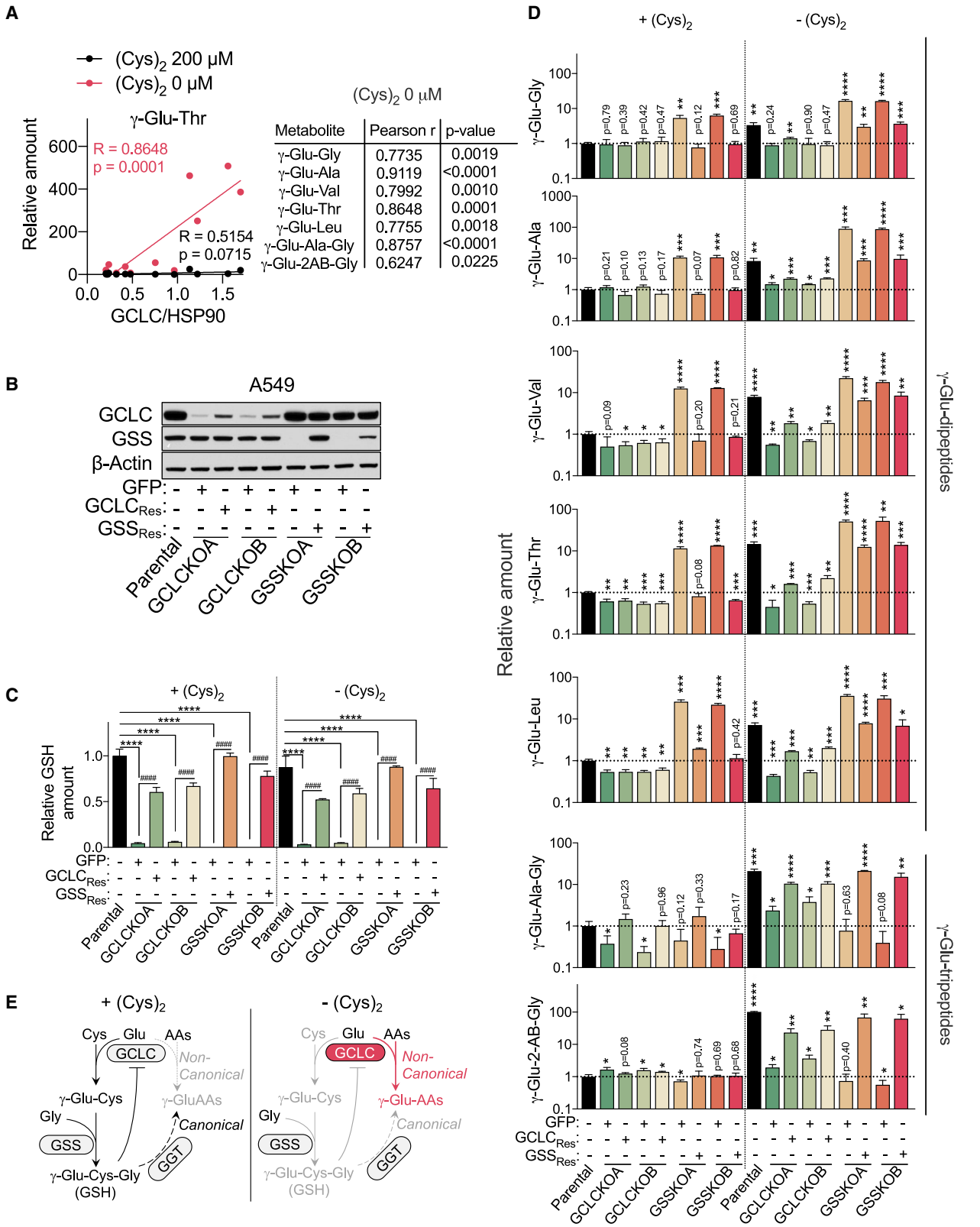

(legend on next page)

Please cite this article in press as: Kang et al., Non-canonical Glutamate-Cysteine Ligase Activity Protects against Ferroptosis, Cell Metabolism (2020), https://doi.org/10.1016/j.cmet.2020.12.007

To directly evaluate the production of γ-glutamyl-dipeptides by GCLC, we generated both GCLC and GSS knockout (KO) A549 clones using CRISPR/Cas9. In both cases, the clones should be deficient in GSH synthesis, but only GCLC KO cells should lack direct γ-glutamyl-dipeptide synthesis capacity. Two clones were generated for both GCLC and GSS KO cells and reconstituted with sgRNA-resistant cDNAs ($GCLC_{Res}$ and GSS_{Res}) to control for any clonal effects during selection (Figure 3B). Importantly, both clones were defective in GSH synthesis as evidenced by significantly reduced intracellular GSH levels compared to parental cells (Figure 3C). However, while the GSS KO clones lacked detectable GSS protein and GSH, the GCLC KO clones were hypomorphic, with a small amount of residual GCLC expression and GSH. Despite repeated attempts, clones completely deficient for GCLC could not be obtained. However, despite this limitation, GCLC KO clones were dramatically impaired in γ-glutamyl-dipeptide accumulation following cystine starvation (Figure 3D). In contrast, GSS KO clones instead had increased γ-glutamyl-dipeptide levels under both fed and starved conditions, although their levels were enhanced by cystine starvation. This is likely explained by the feedback inhibition of GCLC by GSH, and more weakly by γ-Glu-2AB-Gly (Richman and Meister, 1975), which cannot be synthesized in GSS KO cells, leading to hyperactivation of GCLC. The production of γ-Glu-2AB-Gly and γ-Glu-Ala-Gly tripeptides required both GCLC and GSS, because GSS activity is required for the ligation of glycine. These phenotypes were all rescued by the reconstitution of KO cells with sgRNA-resistant cDNAs, confirming the specificity of the KO. Consistent alterations of GSH and γ-glutamyl-peptides were also observed in polyclonal GCLC and GSS KO H1299 cells, which were also rescued by GCLC or GSS restoration (Figures S3A–S3C). The accumulation of γ-glutamyl-peptides following erastin treatment or cystine starvation was also blocked by co-treatment with the GCLC inhibitor buthionine sulfoximine (BSO; Figures S3D–S3F), demonstrating that the enzyme activity of GCLC was necessary for their accumulation. These results indicate that γ-glutamyl-dipeptides are directly generated by GCLC under cystine-starved conditions (Figure 3E).

GCLC Mediates γ-Glutamyl-Peptide Synthesis *In Vivo*

Next, we examined whether GCLC mediates the synthesis of γ-glutamyl-peptides *in vivo* under normal physiological conditions. To this end, mice were treated with a single dose of PBS or cyst(e)inase to deplete serum cystine for 24 h, followed by saline or BSO to inhibit Gclc for 4 h (Figure 4A). In a separate experiment, systemic Gclc deletion was induced in an adult mouse to achieve chronic Gclc inhibition for 2 weeks, which was verified by loss of mRNA expression in the lung, liver, and kidney (Figure 4B). The consequences of these two independent perturbations were examined in these three tissues and the serum. While glutathione and cystine were present in their reduced forms (GSH, Cys) in tissues, the serum had predominantly the oxidized form (GSSG, Cys_2), which may be due to either the oxidizing extracellular conditions or oxidation during sample preparation. Cyst(e)inase effectively depleted cyst(e)ine in the serum (Figure 4C), liver (Figure 4F), and lung (Figure S4A), but unexpectedly elevated cysteine in the kidney (Figure S4D). Cyst(e)ine depletion was accompanied by a modest decrease in liver, kidney, and lung GSH (Figures 4G, S4B, and S4E), but elevated serum GSSG (Figure 4D). As expected, BSO robustly depleted tissue GSH (Figures 4G, S4B, and S4E) and serum GSSG (Figure 4D). Interestingly, BSO did not significantly influence cysteine levels in most tissues (Figures 4F, S4A, and S4D), but did significantly elevate serum $(Cys)_2$ (Figure 4C), possibly as a consequence of impaired GSH synthesis. In addition, the efficacy of Gclc deletion was evident by the depletion of glutathione by 75%–90% in the serum and tissues (Figures 4I, 4K, S4G, and S4I). As observed in cell culture, cysteine depletion elevated the levels of γ-glutamyl-peptides, particularly in the serum and liver, which was reversed by BSO (Figures 4E, 4H, S4C, and S4F). Furthermore, we found that inhibition of Gclc with BSO or enzyme deletion depleted the basal levels of γ-glutamyl-peptides, including both the dipeptides and tripeptides, in all tissues (Figures 4E, 4H, 4J, 4L, S4C, S4F, S4H, and S4J). Overall, these results indicate that GCLC mediates the *in vivo* synthesis of γ-glutamyl-peptides, which is responsive to cysteine availability.

NRF2 Promotes γ-Glutamyl-Peptide Synthesis via GCLC

NSCLC cell lines demonstrated a wide range in the degree of γ-glutamyl-peptide accumulation (Figure 2D), despite similar depletion of intracellular cysteine following cystine starvation (Figure 1E), suggesting additional regulatory mechanisms may explain their levels. We examined the expression of GCLC protein across the NSCLC panel and found the expression of GCLC, and its modifier subunit GCLM, but not GSS, were associated with high activity of NRF2 (Figure 5A), a known regulator of both GCLC and GCLM expression. Consistently, KEAP1 mutant NSCLC cell lines had significantly higher levels of γ-glutamyl-peptides following cystine starvation compared to KEAP1 wild-type cell lines (Figures 5B and S5A). To directly assay the effect

Figure 3. GCLC Mediates γ-Glutamyl-Peptide Synthesis in Cell Culture

(A) Correlation of γ-Glu-dipeptides (data from Figure 2D) with GCLC expression in NSCLC cell lines. The GCLC protein expression of each cell line was normalized to the amount of HSP90 protein. The western blot can be found in Figure 5A.

(B) Representative immunoblots of parental A549 cells, GCLC KO clones reconstituted with GFP (+GFP) or sgRNA-resistant GCLC (+$GCLC_{Res}$), and GSS KO clones reconstituted with GFP (+GFP) or sgRNA-resistant GSS (+GSS_{Res}). β-actin was used for the loading control.

(C and D) Intracellular GSH levels (C) and γ-Glu-peptide levels (D) in the cells from (B) under cystine-replete or -starved conditions for 2.5 h (N = 3). The data were normalized to the mean value of parental A549 cells under cystine-replete conditions.

(E) Schematic depicting the non-canonical, γ-Glu-peptide synthesis activity of GCLC.

For (C) and (D), data are presented as mean ± SD. n.d., not detected. N is number of biological replicates. $^{*}p < 0.05$, $^{**}p < 0.01$, $^{***}p < 0.001$, and $^{****}p < 0.0001$; $^{\#\#}p < 0.01$, $^{\#\#\#}p < 0.001$, $^{\#\#\#\#}p < 0.0001$. For (C), a one-way ANOVA with Bonferroni's multiple comparison test was used for statistical analyses for the comparison of parental, GCLC KOA/B + GFP, and GSS KOA/B + GFP. For the comparison between GCLC KO or GSS KO group (GCLC KOA/B + GFP or GSS KOA/B + GFP) and their GCLC or GSS reconstituted group (GCLC KOA/B + $GCLC_{Res}$ or GSSKO A/B + GSSKOA/B + GSS_{Res}), an unpaired two-tailed t test was used. For (D), an unpaired two-tailed t test was used for the comparison with parental cells under cystine-replete conditions (+$(Cys)_2$).

Please cite this article in press as: Kang et al., Non-canonical Glutamate-Cysteine Ligase Activity Protects against Ferroptosis, Cell Metabolism (2020), https://doi.org/10.1016/j.cmet.2020.12.007

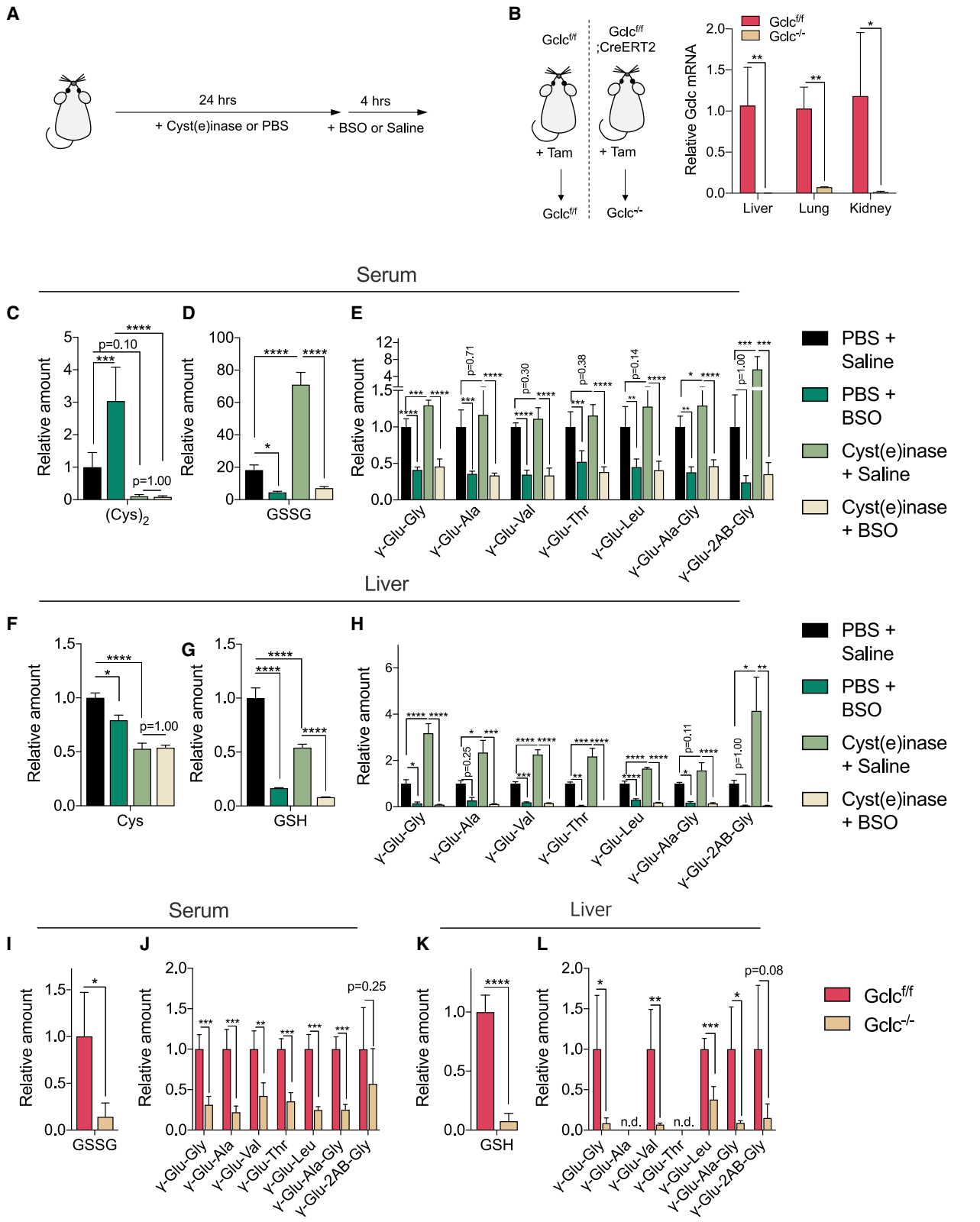

(legend on next page)

Please cite this article in press as: Kang et al., Non-canonical Glutamate-Cysteine Ligase Activity Protects against Ferroptosis, Cell Metabolism (2020), https://doi.org/10.1016/j.cmet.2020.12.007

of NRF2 on GCLC expression and γ-glutamyl-peptide synthesis, we used NRF2 KO A549 cells reconstituted with empty vector or NRF2, which we previously used to study cysteine metabolism (Kang et al., 2019). NRF2 reconstitution in this system led to elevated expression of both GCLC and GCLM (Figure 5C), and significantly increased levels of γ-glutamyl-dipeptides and γ-Glu-2AB-Gly, but not γ-Glu-Ala-Gly, under cystine-starved conditions (Figure 5D), which was inhibited by BSO. In contrast, NRF2 promoted an increase in GSH under cystine-replete conditions (Figure 5E). These results were recapitulated by NRF2 activation in the KEAP1 wild-type cell line Calu3 with the KEAP1 inhibitor KI-696 (Figures 5F–5H) (Davies et al., 2016). Collectively, these results demonstrate that the regulation of GCLC by NRF2 promotes GSH synthesis under cystine-replete conditions, but γ-glutamyl-peptide synthesis under cystine-starved conditions.

Dipeptide Synthesis Protects KEAP1 Mutant Cells from Ferroptosis

We next examined whether γ-glutamyl-peptides play a causal role in protection against ferroptosis. While we found that GCLC expression was anticorrelated with ferroptosis (Figure 6A), exogenous γ-Glu-Ala, γ-Glu-Leu, γ-Glu-Val, or γ-Glu-Gly did not protect GCLC KO A549 cells against cystine starvation-induced ferroptosis (Figure 6B), despite robust uptake of these dipeptides into the cells (Figure S6A). Multiple studies have demonstrated a potent, synergistic effect of the GCLC inhibitor BSO with limitation of cystine uptake or availability (Badgley et al., 2020; Cramer et al., 2017; Harris et al., 2015), leading us to hypothesize it was the synthesis of the γ-glutamyl-peptides, rather than the peptides themselves, that was protective. Indeed, we observed that BSO treatment consistently promoted ferroptosis of the KEAP1 mutant cell lines under cystine starvation but did not significantly affect most KEAP1 wild-type lines (Figures 6C and S6B). We directly tested the effect of NRF2 on ferroptosis by reintroducing NRF2 into NRF2 KO A549 cells, which dramatically suppressed cystine starvation-induced ferroptosis; this effect was partially rescued by GCLC inhibition with BSO (Figure 6D). Similarly, KEAP1 inhibition in KEAP1 wild-type Calu3 cells suppressed cystine starvation-induced ferroptosis, which was completely rescued by BSO (Figure 6E). Because we found that GSH synthesis is dramatically impaired under cystine starvation (Figures 1F and 2B), these results suggest that BSO promotes ferroptosis by inhibiting γ-glutamyl-peptide synthesis. To directly interrogate the role of the γ-glutamyl-peptide synthesis function of GCLC in ferroptosis protection, we used the GCLC and GSS KO A549 clones (Figure 3B), which are both defective in GSH synthesis. Importantly, the GCLC KO clones demonstrated accelerated ferroptosis induction under cystine starvation compared to parental cells, which could be rescued by GCLC cDNA, while the GSS KO clones did not (Figure 6F). Similar results were observed following treatment with the xCT inhibitor erastin (Figure 6G). Furthermore, BSO treatment induced ferroptosis in the GSS KO clones (Figure 6H), but did not further sensitize the GCLC KO clones, further confirming the GSH-independent role of GCLC in ferroptosis protection and the specificity of BSO for GCLC. Finally, both GCLC KO and GSS KO accelerated ferroptosis induction under cystine starvation following acute deletion in KEAP1 wild-type H1299 cells, although GCLC KO was more potent (Figure 6I), suggesting NRF2 activation state may decrease cellular reliance on GSH for ferroptosis protection. Interestingly, we observed KEAP1 wild-type cell lines had higher GPX4 expression, suggesting they may be more reliant on GSH for lipid peroxide detoxification (Figure S6C). Together, these data indicate that GCLC has an additional, GSH-independent function to prevent cystine starvation-induced ferroptosis of NSCLC cells.

Dipeptide Synthesis Scavenges Glutamate

The γ-glutamyl-peptides all have glutamate in common but contain other amino acids that may play a causal role in ferroptosis. To examine this possibility, we examined the association of their levels under cystine starvation with ferroptosis sensitivity. We found that glutamate levels, but not the levels of the other amino acids within γ-glutamyl-peptides, were strongly correlated with ferroptosis (Figure 7A). Importantly, prior work from Papagiannakopoulos and colleagues demonstrated that activation of NRF2 increases the consumption of glutamate for both glutathione synthesis and glutamate secretion by x_c^- antiporter system, thereby limiting glutamate availability for biosynthetic reactions (Sayin et al., 2017). As expected, while there was substantial heterogeneity in the expression of the glutamine transporter SLC1A5 and the glutamate transaminase GOT1 across NSCLC cell lines, we observed that cell lines with high NRF2 levels had high xCT expression and elevated glutamate export under cystine-replete, but not starved, conditions (Figures S7A and S7B). Furthermore, we observed a positive correlation between xCT expression and glutamate export only under

Figure 4. GCLC Mediates γ-Glutamyl-Peptide Synthesis *In Vivo*

(A) Schematic depicting the Cyst(e)inase and BSO treatment schedule for the depletion of extracellular cyst(e)ine and inhibition of Gclc. Cyst(e)inase (75 mg/kg) or vehicle (PBS) was administered, followed by treatment with BSO (10 mmol/kg) or vehicle (saline) 24 h later. Tissues were collected after 4 h.

(B) Evaluation of Gclc mRNA expression after tamoxifen (Tam)-inducible Gclc deletion in the adult mouse. $Gclc^{f/f}$ (control, Gclc functional) and $Gclc^{-/-}$ (Gclc knockout). The mRNA levels are normalized to the mean value of $Gclc^{f/f}$ mouse tissues (N = 4).

(C–E) Analysis of serum cystine (C), GSSG (D), and γ-Glu-peptide levels (E) in mice treated with cyst(e)inase/BSO.

(F–H) Analysis of liver cysteine (F), GSH (G), and γ-Glu-peptide levels (H) in the mice from (C)–(E). The metabolite levels are normalized to the mean value of PBS/saline-treated mice (N = 5).

(I and J) Analysis of serum GSSG (I) and γ-Glu-peptide levels (J) in $Gclc^{f/f}$ and $Gclc^{-/-}$ mice.

(K and L) Analysis of liver GSH (K) and γ-Glu-peptide levels (L) in the mice from (I) and (J). The metabolite levels are normalized to the mean value of $Gclc^{f/f}$ mice (N = 4).

For (B)–(L), data are presented as mean ± SD. N is number of biological replicates. n.d., not detected. *$p < 0.05$, **$p < 0.01$, ***$p < 0.001$, and ****$p < 0.0001$. For (B) and (I)–(L), an unpaired two-tailed t test was used for the statistical comparisons. For (C)–(H), a one-way ANOVA with Bonferroni's multiple comparison test was used for statistical analyses.

Please cite this article in press as: Kang et al., Non-canonical Glutamate-Cysteine Ligase Activity Protects against Ferroptosis, Cell Metabolism (2020), https://doi.org/10.1016/j.cmet.2020.12.007

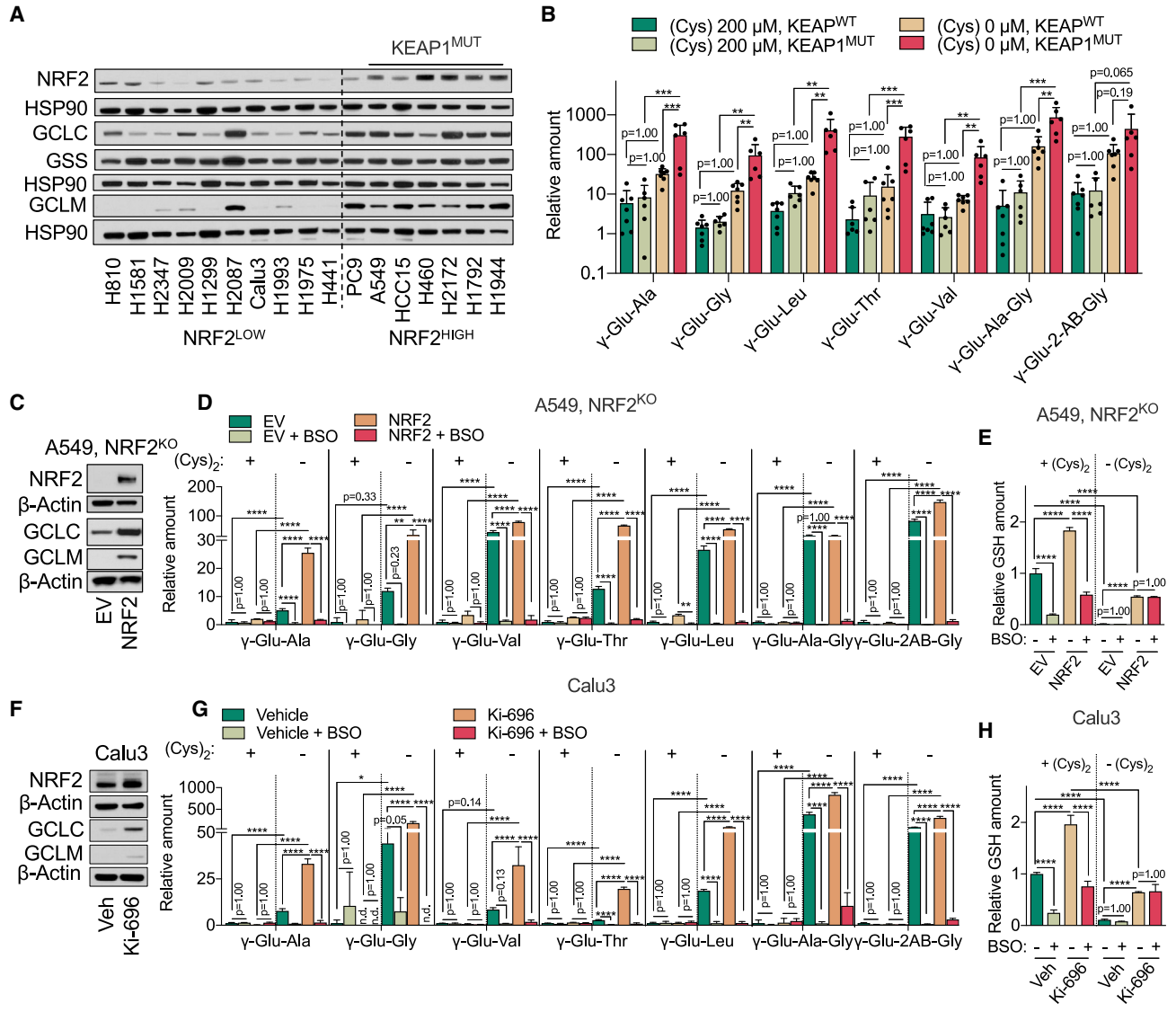

Figure 5. NRF2 Promotes γ-Glutamyl-Peptide Synthesis via GCLC

(A) Representative immunoblot of NRF2, GCLC, GSS, and GCLM expression in NRF2^{LOW} and NRF2^{HIGH} (KEAP1 mutant: A549, HCC15, H460, H2172, H1792, and H1944) NSCLC cell lines. HSP90 is used as loading control.

(B) Comparison of γ-Glu-peptide levels in KEAP1^{WT} and KEAP^{MUT} NSCLC cell lines. Individual cell line data are found in Figure S5A, and also correspond to the data in Figure 2D. The γ-Glu-peptides were analyzed following culture in cysteine-replete and -starved conditions for 12 h and normalized to the mean value of H1581 cells under cystine-replete conditions.

(C) Representative immunoblot of NRF2, GCLC, and GCLM expression in NRF2 KO A549 cells transduced with empty vector (EV) or NRF2. β-actin is used as loading control.

(D and E) Analysis of intracellular γ-Glu-peptides (D) and GSH levels (E) in the cells from (C) under cystine-replete or -starved conditions in the presence and absence of 100 μM BSO for 12 h.

(F) Representative immunoblot of NRF2, GCLC, and GCLM expression in Calu3 cells pre-treated with 100 nM KI-696 or vehicle (Veh, 0.1% DMSO) for 48 h. β-actin is used as loading control.

(G and H) Analysis of intracellular γ-Glu-peptide (G) and GSH levels (H) in the cells from (F) under cystine-replete or -starved conditions in the presence and absence of 100 μM BSO for 12 h.

For (B), (D), (E), (G), and (H), data are presented as mean ± SD. N is number of biological replicates. n.d., not detected. **p < 0.01, ***p < 0.001, and ****p < 0.0001. For (B), (D), (E), (G), and (H), a one-way ANOVA with Bonferroni's multiple comparison test was used for statistical analyses.

cystine-replete conditions (Figure 7B). In contrast, GCLC protein levels and intracellular glutamate were anticorrelated under both cystine-replete and -starved conditions (Figure 7C), suggesting that GCLC was still capable of limiting intracellular glutamate in the absence of cysteine. Furthermore, we observed that KEAP1 mutant cells had lower intracellular levels of glutamate, but not glycine (Figure S7C), which was preserved under cystine-starved conditions (Figure 7D).

Please cite this article in press as: Kang et al., Non-canonical Glutamate-Cysteine Ligase Activity Protects against Ferroptosis, Cell Metabolism (2020), https://doi.org/10.1016/j.cmet.2020.12.007

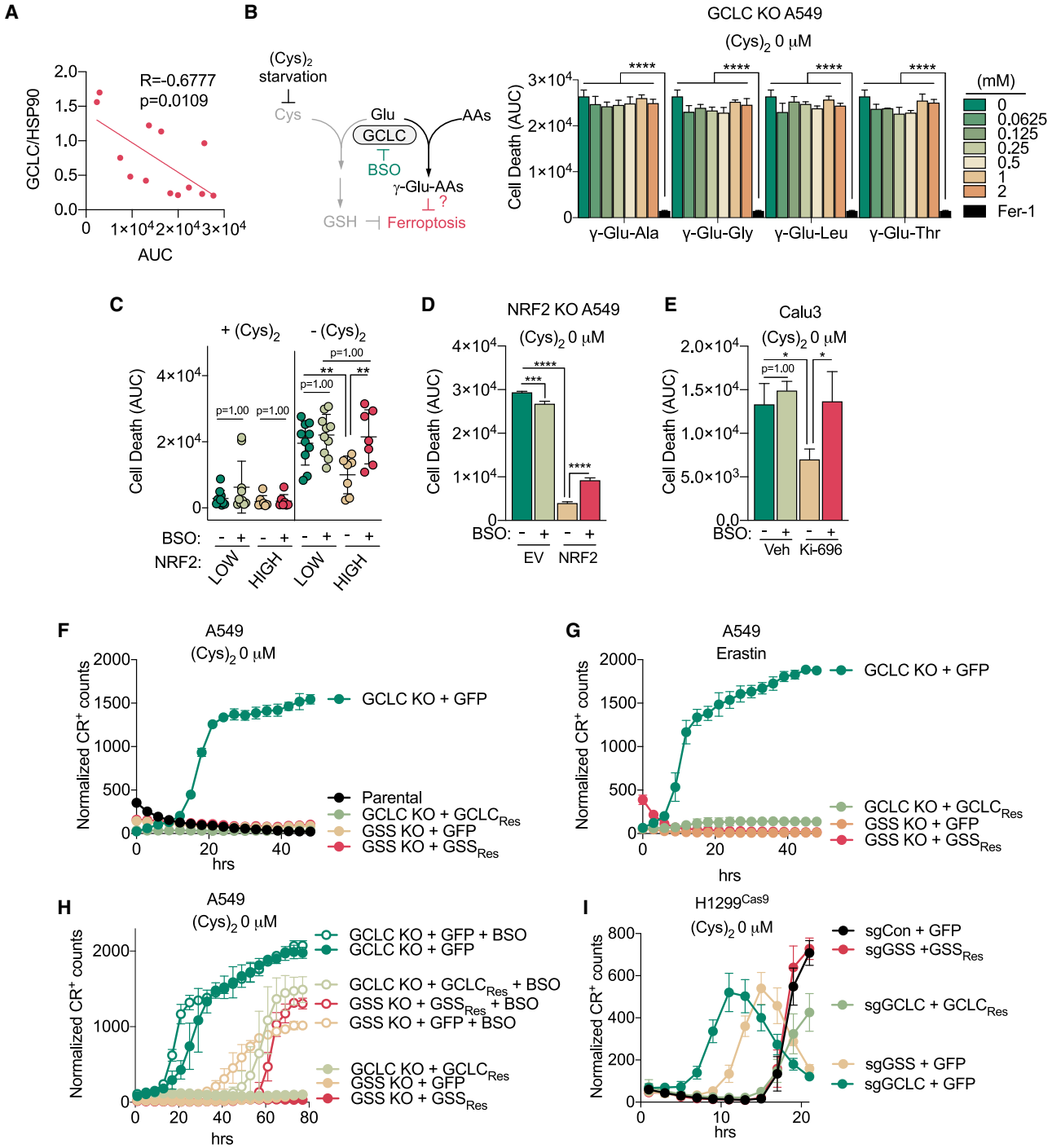

Figure 6. Dipeptide Synthesis Protects KEAP1 Mutant Cells from Ferroptosis

(A) Correlation between cell death under cystine starvation (AUC, from Figure 1A) and GCLC expression in NSCLC cells (N = 13). GCLC expression is normalized to HSP90 expression and can be found in Figure 5A.

(B) Evaluation of the influence of γ-Glu-dipeptide treatment on the death of GCLC KO A549 cells under cystine starvation. Cells were treated with γ-Glu-dipeptides at the indicated concentration or Fer-1 (10 μM) as a positive control. Cell death was monitored with Sytox Green every 2 h for 49 h, normalized to cell density, and then AUCs were calculated (N = 3).

(C) Evaluation of the death of $NRF2^{HIGH}$ (N = 7) and $NRF2^{LOW}$ (N = 10) cell lines under cysteine-replete and -starved conditions in the presence and absence of 100 μM BSO. Each dot represents the mean AUC of each NSCLC cell line. Cell death was monitored with Sytox Green and individual cell line data are found in Figure S6B.

(D) Evaluation of the death of NRF2 KO A549 cells transduced with empty vector (EV) or NRF2 under cystine-replete and -starved conditions in the presence and absence of 100 μM BSO (N = 3). Cell death was monitored by Sytox Green every 2 h for 65 h, followed by AUC calculation.

(legend continued on next page)

Please cite this article in press as: Kang et al., Non-canonical Glutamate-Cysteine Ligase Activity Protects against Ferroptosis, Cell Metabolism (2020), https://doi.org/10.1016/j.cmet.2020.12.007

To directly evaluate whether NRF2 influences glutamate levels under cystine starvation, we used the NRF2 KO A549 cell system, which exhibited increased GCLC-dependent γ-glutamyl-dipeptide synthesis upon NRF2 reconstitution (Figure 5D). NRF2 expression reduced intracellular glutamate under both cystine-replete and -starved conditions, which was partially reversed by GCLC inhibition with BSO (Figure 7E). Similar results were observed in the KEAP1 wild-type cell line Calu3 (Figure 7F). Moreover, treatment of A549 cells with BSO promoted glutamate accumulation following erastin-mediated xCT inhibition (Figure S7D). Next, we evaluated the ability of γ-glutamyl-dipeptides to serve as a glutamate sink. GCLC KO A549s demonstrated increased intracellular glutamate levels under cystine starvation, while GSS KO A549s did not (Figure 7G), which was also observed in H1299s to a lesser degree (Figure S7E). Finally, GCLC KO liver dramatically accumulated glutamate, with a similar trend observed in wild-type livers following a single treatment of BSO, even under cysteine-limiting conditions (Figure 7H). Together, these results demonstrate that dipeptide synthesis via GCLC serves as a glutamate sink to limit glutamate accumulation under cystine starvation.

Because glutamate was previously shown to contribute to ferroptosis (Dixon et al., 2012; Gao et al., 2015), we examined whether glutamate plays a causal role in cystine starvation-induced ferroptosis in NSCLC cells. We depleted intracellular glutamate by starving cells of glutamine, or inhibited glutamate metabolism to α-ketoglutarate by treatment with the pan transaminase inhibitor AOA. While glutamine starvation depleted intracellular glutamate, α-ketoglutarate, and downstream metabolites like succinate, AOA treatment elevated glutamate while depleting downstream metabolites (Figure S7F). To elevate intracellular glutamate, cells were treated with membrane-permeable glutamate diethyl ester (GluEE) at 5 mM, a concentration we confirmed could increase intracellular glutamate (Figure S7G). GluEE did not inhibit xCT activity, unlike glutamate itself, which was a potent xCT inhibitor (Figure S7H). Glutamine starvation and AOA treatment could both mitigate ferroptosis independent of NRF2 expression status, while GluEE treatment promoted ferroptosis in most $NRF2^{HIGH}$ cell lines, but not $NRF2^{LOW}$ cell lines (Figures 7I and S7I). Moreover, cystine starvation-induced ferroptosis of GCLC KO cells was rescued by glutamine starvation, which was further enhanced by co-starvation of glutamate (Figure S7J). Glutamate was previously shown to promote ROS accumulation following cystine starvation in multiple studies. Using the general oxidative stress indicator CellROX green, we found that cystine starvation promoted ROS accumulation, which was rescued by glutamine starvation and AOA treatment (Figure 7J) and exacerbated by GluEE treatment (Figure 7K). However, while some studies suggest that glutamate promotes mitochondrial ROS via the electron transport chain (Gao et al., 2015, 2019), others have demonstrated that the mitochondria are dispensable for glutamate-induced ferroptosis (Dixon et al., 2012; Gaschler et al., 2018). Using MitoSOX, we found that cystine starvation did not increase mitochondrial superoxide, consistent with the observations of Dixon et al. (Figure S7K), suggesting mitochondria-derived superoxide is likely not the source of glutamate-induced ROS in our system. Collectively, these results suggest that glutamate promotes ROS accumulation, but the precise mechanism remains to be determined and requires future study.

DISCUSSION

The findings reported herein demonstrate that γ-glutamyl-peptide synthesis by GCLC provides GSH-independent protection from cystine starvation-induced ferroptosis in cells with NRF2 activation. NRF2 has previously been linked to ferroptosis protection (Fan et al., 2017; Sun et al., 2016), and many of its targets have canonical functions that are protective against cellular oxidation, including those promoting glutathione synthesis, ROS metabolism, iron metabolism, and others. The ability of NRF2 to protect against ferroptosis has important implications for cancer, particularly lung cancers that commonly have NRF2 activation via mutations in KEAP1 and NRF2 (Hayes and McMahon, 2009). Further work is needed to determine whether NRF2 protects against specific classes of ferroptosis inducers *in vivo*. Moreover, the contribution of the non-canonical function of GCLC versus other NRF2-regulated processes to protection against these specific classes of ferroptosis inducers remains to be explored.

While cystine starvation-induced ferroptosis has commonly been attributed to the depletion of cellular GSH, we show that cystine starvation induces complex metabolic changes within cells. Our work does not exclude the importance of GCLC-derived GSH in the protection against ferroptosis. GSH is a major intracellular antioxidant and substrate for GPX4 for lipid hydroperoxide detoxification (Dixon and Stockwell, 2019; Yang et al., 2014). However, our work demonstrates that cystine starvation causes a metabolic imbalance and accumulation of glutamate, which plays a causal role in ferroptosis induction. Our findings are consistent with prior reports demonstrating that glutamate contributes to ferroptosis via ROS (Dixon et al.,

(E) Evaluation of the death of Calu3 cells pre-treated with 100 nM of KI-696 or vehicle (Veh, 0.1% DMSO) for 48 h, followed by culture under cystine-replete and -starved conditions in the presence and absence of 100 μM BSO (N = 3). Cell death was monitored with Sytox Green every 2 h for 47 h, followed by AUC calculation.

(F) Evaluation of the death of parental A549 cells, GCLC KO clones reconstituted with GFP (+GFP) or sgRNA-resistant GCLC ($+GCLC_{Res}$), and GSS KO clones reconstituted with GFP (+GFP) or sgRNA-resistant GSS ($+GSS_{Res}$) following cystine starvation for the indicated time points (N = 3).

(G) Evaluation of the death of GCLC KO clones reconstituted with GFP (+GFP) or sgRNA-resistant GCLC ($+GCLC_{Res}$), and GSS KO clones reconstituted with GFP (+GFP) or sgRNA-resistant GSS ($+GSS_{Res}$) treated with Erastin (5 μM) for the indicated time points (N = 3).

(H) Evaluation of the death of the cells from (G) under the cystine-starved conditions in the presence and absence of 100 μM BSO (N = 3).

(I) Evaluation of the death of $H1299^{Cas9}$ cells infected with sgRNAs (sgCon, sgGCLC, or sgGSS), followed by reconstitution with GFP (+GFP), sgRNA-resistant GCLC ($+GCLC_{Res}$), or sgRNA-resistant GSS ($+GSS_{Res}$) under cystine-starved conditions (N = 4).

For (F)–(H), results are representative of two independent GCLC and GSS KO clones. For (F)–(I), cell death was monitored by Cytotox Red (CR) every 2 (I), 3 (F and G), or 4 h (H). For (B)–(I), data are presented as mean ± SD. N is number of biological replicates. *$p < 0.05$, ***$p < 0.001$, and ****$p < 0.0001$. For (A), a Pearson correlation analysis was used. For (B)–(E), a one-way ANOVA with Bonferroni's multiple comparison test was used for statistical analyses.

Please cite this article in press as: Kang et al., Non-canonical Glutamate-Cysteine Ligase Activity Protects against Ferroptosis, Cell Metabolism (2020), https://doi.org/10.1016/j.cmet.2020.12.007

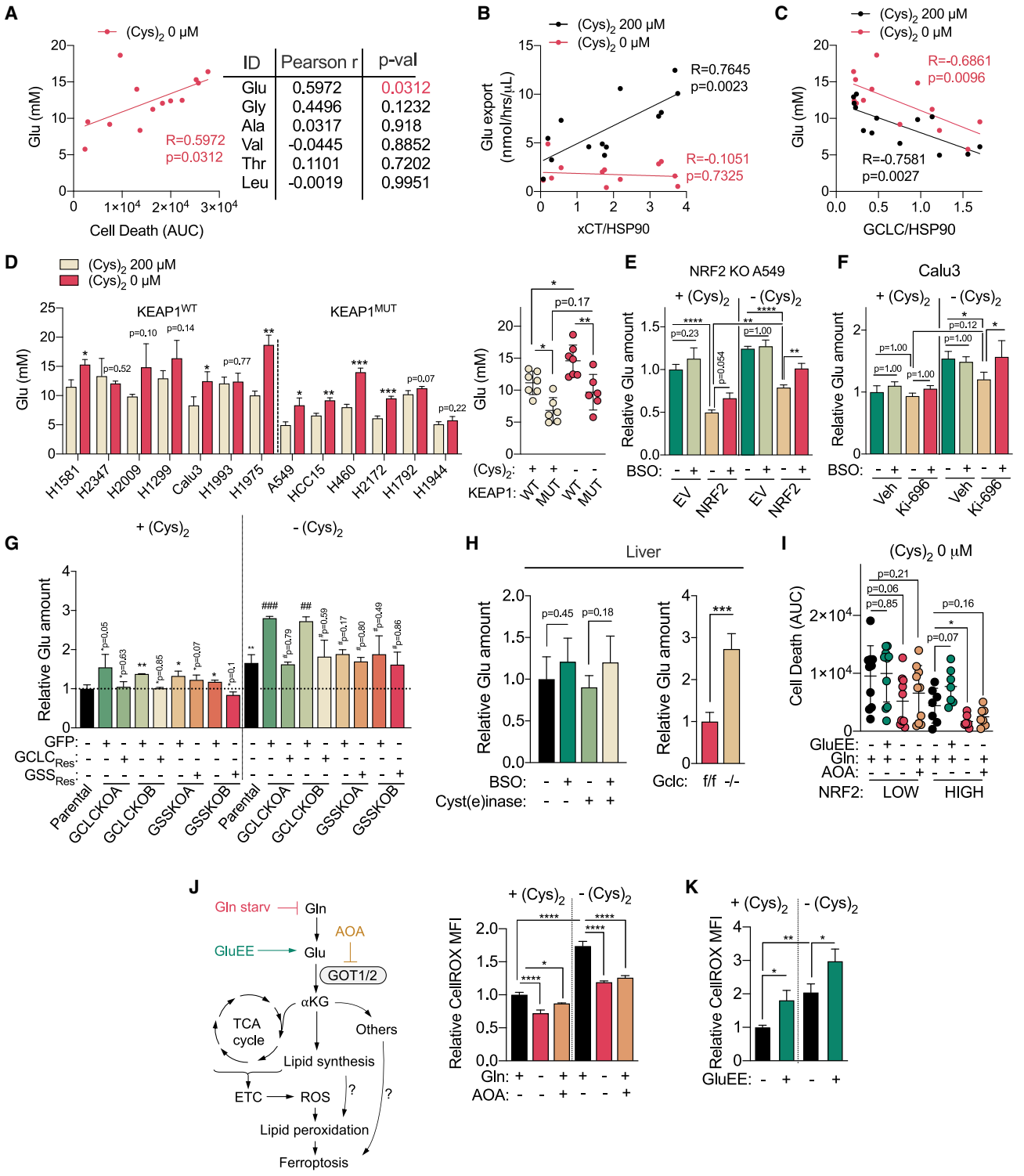

Figure 7. Dipeptide Synthesis Scavenges Glutamate

(A) Correlation between the intracellular concentrations of γ-Glu-peptide substrate amino acids (Glu, Gly, Ala, Val, Thr, and Leu) following cystine starvation for 12 h and cystine starvation AUCs (from Figure 1A) (N = 13). Individual cell line Glu concentrations can be found in (D).

(B) Correlation between xCT protein expression and the Glu export rate under cystine-replete and -starved conditions for 12 h in NSCLC cells. xCT expression is normalized to HSP90 expression and can be found in Figure S7A (N = 13).

(C) Correlation between GCLC protein expression and intracellular Glu levels in NSCLC cell lines cultured in cysteine-replete and -starved conditions for 12 h. GCLC expression is normalized to HSP90 expression and can be found in Figure 5A (N = 13).

(legend continued on next page)

Please cite this article in press as: Kang et al., Non-canonical Glutamate-Cysteine Ligase Activity Protects against Ferroptosis, Cell Metabolism (2020), https://doi.org/10.1016/j.cmet.2020.12.007

2012; Gao et al., 2015, 2019), although more work is needed to understand the mechanism. Glutamate-derived α-ketoglutarate can contribute to fatty acid metabolism via citrate, and lipid metabolism plays a key role in ferroptosis susceptibility (reviewed in Zou and Schreiber, 2020). Moreover, recent work has established an important role for amino acid levels in ferroptosis sensitivity through mTOR-dependent and independent mechanisms (Conlon et al., 2019). More work is needed to understand the signaling effects of glutamate on ferroptosis sensitivity.

Previous studies have found that combined inhibition of cystine uptake with glutathione synthesis can synergistically inhibit the viability of cells and tumors (Cramer et al., 2017; Harris et al., 2015). Our work has important implications for the interpretation of studies using BSO to inhibit GCLC. While many of those results may be attributed to GSH depletion, the contribution of GCLC to γ-glutamyl-peptide synthesis and glutamate scavenging may also play a very important role, particularly in the context of xCT inhibition, where cells cannot export glutamate. Our findings warrant the development of potent GSS inhibitors for the study of ferroptosis to distinguish these mechanisms. These inhibitors would also be valuable for therapeutic combinations with ferroptosis inducers, although they may increase glutamate scavenging, which may affect cellular responses.

Our *in vivo* results provide direct genetic evidence to support the GCLC-mediated γ-glutamyl-peptide production that was recently reported in mouse liver extracts (Kobayashi et al., 2020), where glutamate could be ligated with other amino acids in a reaction inhibited by BSO. The promiscuity of GCLC toward amino acids other than cysteine is not a unique feature of this enzyme and has been shown for many other metabolic enzymes. For example, serine palmitoyl transferase will also metabolize alanine or glycine when serine is limiting (Penno et al., 2010) and glutamate-aspartate aminotransferase will also metabolize cysteine sulfinic acid (Weinstein et al., 1988). In the case of GCLC, this feature may have been selected for during evolution, as the *S. cerevisiae* homolog (Gsh1p) also has the ability to at least use valine (Sofyanovich et al., 2019). Additional work is needed to determine which other amino acids are accepted by *S. cerevisiae* Gsh1p. For the human enzyme, small, non-charged amino acids that are structurally similar to cysteine can be used based on their appearance in γ-glutamyl-peptides, although the full spectrum of amino acids has not been tested in a direct enzymatic assay.

Our findings may extend beyond conditions of cysteine deficiency. Systemic deletion of mouse *Gclc* revealed that Gclc plays a role in the regulation of glutamate and γ-glutamyl-peptide levels in normal tissue. Notably, glutamate accumulation was only observed in the liver, but not other tissues (data not shown). Liver plays a critical role in GSH synthesis to supply the rest of the organism, which may consume significantly more glutamate in liver than lung or kidney (Ookhtens and Kaplowitz, 1998). Similar to the liver, cancer cells synthesize a significant amount of GSH (Balendiran et al., 2004; Huang et al., 2001; Soini et al., 2001; Sun et al., 2019; Tatebe et al., 2002) and use glutamate for cystine export (Ji et al., 2018; Shin et al., 2017; Takeuchi et al., 2013; Timmerman et al., 2013), which may explain the robust accumulation of glutamate following cystine starvation in our NSCLC cells. It is important to note that, in contrast to cell culture, depletion of γ-glutamyl-peptides in Gclc KO tissue may be a consequence of both canonical, extracellular GGT-mediated γ-glutamyl-dipeptide production and the intracellular GCLC-mediated pathway. However, the accumulation of glutamate and the depletion of γ-glutamyl-tripeptides, which require the activity of GSS, strongly suggest that these peptides are being produced intracellularly. Supportively, the activity of GGT is negligible in the mouse liver compared to kidney (Kobayashi et al., 2020). It is not known whether γ-glutamyl-peptides have additional functions in tissues beyond serving as a reservoir for glutamate and potentially other amino acids. γ-glutamyl-peptide levels have been shown to be increased under conditions of liver injury, including drug-induced injury, hepatitis infection, liver cirrhosis, and hepatocellular carcinoma (Soga et al., 2011). Additional work is needed to understand the role of γ-glutamyl-peptide synthesis in these diseases.

We also find that GSS may regulate glycine homeostasis by producing γ-glutamyl-tripeptides, including γ-Glu-2AB-Gly and γ-Glu-Ala-Gly. While we found that glycine also accumulated following cystine starvation (Figure S7C), this was not associated with ferroptosis (Figure 7A). Future work is needed to both

(D) Left: analysis of intracellular Glu concentrations in NSCLC cell lines cultured under cystine-replete or -starved conditions for 12 h (N = 3). Right: comparison of Glu concentrations between $KEAP1^{WT}$ (N = 7) and $KEAP1^{MUT}$ (N = 6) NSCLC cells.

(E) Analysis of relative intracellular Glu levels in the NRF2 KO A549 cells transduced with empty vector (EV) or NRF2 cultured under cystine-replete or -starved conditions in the presence and absence of 100 μM BSO for 12 h (N = 3).

(F) Analysis of relative intracellular Glu levels in the Calu3 cells pre-treated with 100 nM KI-696 or vehicle (Veh, 0.1% DMSO) for 48 h, followed by culture in cystine-replete or -starved conditions in the presence and absence of 100 μM BSO for 12 h (N = 3).

(G) Analysis of relative intracellular Glu levels of the parental A549 cells, GCLC KO clones reconstituted with GFP (+GFP) or sgRNA-resistant GCLC ($+GCLC_{Res}$), and GSS KO clones reconstituted with GFP (+GFP) or sgRNA-resistant GSS ($+GSS_{Res}$) cultured under cystine-replete or -starved conditions for 2.5 h (N = 3).

(H) Left: relative Glu levels in mouse liver treated with cyst(e)inase or vehicle (PBS) for 24 h followed by treatment with BSO or vehicle (saline) for 4 h (for all exp group, N = 5). Right: relative Glu levels in the liver of $Gclc^{f/f}$ and $Gclc^{-/-}$ mice (for all exp group, N = 4).

(I) Analysis of the death of $NRF2^{LOW}$ (N = 10) and $NRF2^{HIGH}$ (N = 7) cells under cystine-starved conditions treated with GluEE (5 mM) or AOA (0.5 mM), or Gln starvation for 49 h. Cell death was analyzed with Sytox Green and the mean AUC of each cell lines can be found in Figure S7I.

(J) Analysis of intracellular A549 ROS levels with CellROX green following culture under cystine-replete and -starved conditions in the presence and absence of AOA (0.5 mM) or Gln starvation for 14 h (N = 3).

(K) Analysis of intracellular A549 ROS levels with CellROX green following culture under cystine-replete and -starved conditions in the presence and absence of GluEE (5 mM) for 8 h (N = 3).

For (D)–(K), data are presented as mean ± SD. N is number of biological replicates. *$p < 0.05$, **$p < 0.01$, ***$p < 0.001$, and ****$p < 0.0001$. For (A)–(C), a Pearson correlation analysis was used. For (D) (left), (G), (H) (right), and (I), unpaired two-tailed t tests were used for the statistical comparisons. For (G), * is for the comparison with parental cells under cystine-replete conditions ($+(Cys)_2$) and # is for the comparison of parental group under cystine-starved conditions ($-(Cys)_2$). For (D) (right), (E), (F), (H) (left), (J), and (K), one-way ANOVA with Bonferroni's multiple comparison tests was used for statistical analyses.

understand whether GSS can use other amino acids besides glycine and determine the full spectrum of γ-glutamyl-tripeptides produced by GSS. Further, we find that GSS deficiency actually enhances γ-glutamyl-dipeptide synthesis, which can be explained by loss of feedback inhibition of GCLC by GSH. These findings raise interesting implications for the metabolic phenotypes of patients with inborn errors of glutathione metabolism. Although extremely rare, mutations in GCLC and GSS result in hemolytic anemia. Interestingly, GSS mutant patients also present with 5-oxo-prolinuria, which is not observed in GCLC deficiency (Ristoff and Larsson, 2007). While this 5-oxo-prolinuria has been attributed to the accumulation of γ-glutamyl-cysteine and its metabolism to 5-oxo-proline by γ-glutamylcyclotransferase (GGCT) (Ristoff and Larsson, 2007), our work suggests that other γ-glutamyl amino acids are likely produced in this situation to contribute to 5-oxo-prolinuria. This is likely to depend on the availability of cysteine, which would likely become limiting if the feedback inhibition of GCLC is lost due to an inability to synthesize GSH.

Limitations of Study

Although this study demonstrates a non-canonical role for GCLC in ferroptosis protection via glutamate scavenging, the study is limited to NSCLC cells and cystine starvation-induced ferroptosis. The role of glutamate scavenging by GCLC in other cancer types and in response to other ferroptosis inducers remains to be determined. While we provide *in vivo* evidence for γ-glutamyl-peptide synthesis by GCLC and its role in controlling glutamate levels, it will be important to examine this pathway in various tumor models. Finally, as discussed above, more work is needed to understand how glutamate influences ferroptosis.

STAR★METHODS

Detailed methods are provided in the online version of this paper and include the following:

- KEY RESOURCES TABLE
- RESOURCE AVAILABILITY
  - Lead Contact
  - Material Availability
  - Data and Code Availability
- EXPERIMENTAL MODEL AND SUBJECT DETAILS
  - Animal Experiments
- METHOD DETAILS
  - Lentivirus Generation
  - Lentiviral Infection of NSCLC Cells
  - Dead Cell Measurement with IncuCyte
  - Metabolomics Sample Preparation
  - Quantitation of Glutamate Exportation
  - LC-MS Analysis
  - ROS and Lipid Peroxidation Measurements
  - Immunoblotting
- QUANTIFICATION AND STATISTICAL ANALYSIS

SUPPLEMENTAL INFORMATION

Supplemental Information can be found online at https://doi.org/10.1016/j.cmet.2020.12.007.

ACKNOWLEDGMENTS

We would like to thank Dr. Joshua D. Rabinowitz for SHIN-1; Dr. Vince Luca, Dr. David Gonzalez-Perez, Elliot Medina, and Sae Bom Lee for flow cytometry assistance; Dr. Min Liu and Jayden K. Cline for LC-MS assistance; Dr. Joseph O. Johnson, Tingan Chen, Dr. Anna P. Gomes, and Dr. Didem Ilter for Incucyte assistance; and all members of the DeNicola laboratory for their very helpful discussions. This work was supported by grants from the NIH/NCI (R37-CA230042) and NIH/NIDDK (R01-DK123738) to G.M.D., NIH/NCI (CA189623) to E.S., the Ludwig Center at Harvard to I.S.H., the AACR-Takeda Oncology Lung Cancer Research Fellowship (19-40-38-KANG) to Y.P.K., and a National Pancreas Foundation grant to C.J. This work was also supported by Miles for Moffitt funds awarded to the Lung Cancer Metabolism Working Group; the Analytic Microscopy and the Proteomics/Metabolomics Cores, which are funded in part by Moffitt's Cancer Center Support Grant (NCI, P30-CA076292) and grants from the Moffitt Foundation; and a Florida Bankhead-Coley grant (06BS-02–9614) to the Proteomics/Metabolomics core.

AUTHOR CONTRIBUTIONS

Y.P.K. and G.M.D. designed the study and interpreted experimental results. Y.P.K. performed all metabolomics experiments, Y.P.K., A.M.-M., and C.J. performed western blotting experiments; Y.P.K. and A.M.-M. performed cell viability experiments; Y.P.K. and C.J. generated KO cell lines and performed flow cytometry experiments; A.F. and N.P.-F. performed cyst(e)inase/BSO animal experiments; E.S. generated and provided cyst(e)inase; I.S.H. generated Gclc KO mice and collected tissues; Y.P.K. and G.M.D. wrote the manuscript; and all authors commented on it.

DECLARATION OF INTERESTS

I.S.H. is a consultant for Ono Pharma USA. E.S. is an inventor of intellectual property related cyst(e)inase, and has an equity interest in Aeglea Biotherapeutics, a company pursuing the commercial development of cyst(e)inase. These companies had no role in funding or the design of this study.

Received: June 2, 2020
Revised: October 9, 2020
Accepted: December 8, 2020
Published: December 22, 2020

REFERENCES

Alvarez, S.W., Sviderskiy, V.O., Terzi, E.M., Papagiannakopoulos, T., Moreira, A.L., Adams, S., Sabatini, D.M., Birsoy, K., and Possemato, R. (2017). NFS1 undergoes positive selection in lung tumours and protects cells from ferroptosis. Nature *551*, 639–643.

Anderson, M.E. (1998). Glutathione: an overview of biosynthesis and modulation. Chem. Biol. Interact. *111-112*, 1–14.

Badgley, M.A., Kremer, D.M., Maurer, H.C., DelGiorno, K.E., Lee, H.J., Purohit, V., Sagalovskiy, I.R., Ma, A., Kapilian, J., Firl, C.E.M., et al. (2020). Cysteine depletion induces pancreatic tumor ferroptosis in mice. Science *368*, 85–89.

Balendiran, G.K., Dabur, R., and Fraser, D. (2004). The role of glutathione in cancer. Cell Biochem. Funct. *22*, 343–352.

Beatty, P.W., and Reed, D.J. (1980). Involvement of the cystathionine pathway in the biosynthesis of glutathione by isolated rat hepatocytes. Arch. Biochem. Biophys. *204*, 80–87.

Bennett, B.D., Yuan, J., Kimball, E.H., and Rabinowitz, J.D. (2008). Absolute quantitation of intracellular metabolite concentrations by an isotope ratio-based approach. Nat. Protoc. *3*, 1299–1311.

Bersuker, K., Hendricks, J.M., Li, Z., Magtanong, L., Ford, B., Tang, P.H., Roberts, M.A., Tong, B., Maimone, T.J., Zoncu, R., et al. (2019). The CoQ oxidoreductase FSP1 acts parallel to GPX4 to inhibit ferroptosis. Nature *575*, 688–692.

Cao, J.Y., and Dixon, S.J. (2016). Mechanisms of ferroptosis. Cell. Mol. Life Sci. *73*, 2195–2209.

Please cite this article in press as: Kang et al., Non-canonical Glutamate-Cysteine Ligase Activity Protects against Ferroptosis, Cell Metabolism (2020), https://doi.org/10.1016/j.cmet.2020.12.007

Cao, J.Y., Poddar, A., Magtanong, L., Lumb, J.H., Mileur, T.R., Reid, M.A., Dovey, C.M., Wang, J., Locasale, J.W., Stone, E., et al. (2019). A genome-wide haploid genetic screen identifies regulators of glutathione abundance and ferroptosis sensitivity. Cell Rep. *26*, 1544–1556.e8.

Chen, Y., Yang, Y., Miller, M.L., Shen, D., Shertzer, H.G., Stringer, K.F., Wang, B., Schneider, S.N., Nebert, D.W., and Dalton, T.P. (2007). Hepatocyte-specific Gclc deletion leads to rapid onset of steatosis with mitochondrial injury and liver failure. Hepatology *45*, 1118–1128.

Chen, P.H., Cai, L., Huffman, K., Yang, C., Kim, J., Faubert, B., Boroughs, L., Ko, B., Sudderth, J., McMillan, E.A., et al. (2019). Metabolic diversity in human non-small cell lung cancer cells. Mol. Cell *76*, 838–851.e5.

Conlon, M., Poltorack, C., Forcina, G.C., Wells, A., Mallais, M., Kahanu, A., Magtanong, L., Pratt, D.A., and Dixon, S.J. (2019). A compendium of kinetic cell death modulatory profiles identifies ferroptosis regulators. bioRxiv. https://doi.org/10.1101/826925.

Conrad, M., and Friedmann Angeli, J.P. (2015). Glutathione peroxidase 4 (Gpx4) and ferroptosis: what's so special about it? Mol. Cell. Oncol. *2*, e995047.

Cramer, S.L., Saha, A., Liu, J., Tadi, S., Tiziani, S., Yan, W., Triplett, K., Lamb, C., Alters, S.E., Rowlinson, S., et al. (2017). Systemic depletion of L-cyst(e)ine with cyst(e)inase increases reactive oxygen species and suppresses tumor growth. Nat. Med. *23*, 120–127.

Davies, T.G., Wixted, W.E., Coyle, J.E., Griffiths-Jones, C., Hearn, K., McMenamin, R., Norton, D., Rich, S.J., Richardson, C., Saxty, G., et al. (2016). Monoacidic inhibitors of the kelch-like ECH-associated protein 1: nuclear factor erythroid 2-related factor 2 (KEAP1:NRF2) protein-protein interaction with high cell potency identified by fragment-based discovery. J. Med. Chem. *59*, 3991–4006.

DeNicola, G.M., Chen, P.H., Mullarky, E., Sudderth, J.A., Hu, Z., Wu, D., Tang, H., Xie, Y., Asara, J.M., Huffman, K.E., et al. (2015). NRF2 regulates serine biosynthesis in non-small cell lung cancer. Nat. Genet. *47*, 1475–1481.

Dixon, S.J., and Stockwell, B.R. (2019). The hallmarks of ferroptosis. Annu Rev Cancer Biol *3*, 35–54.

Dixon, S.J., Lemberg, K.M., Lamprecht, M.R., Skouta, R., Zaitsev, E.M., Gleason, C.E., Patel, D.N., Bauer, A.J., Cantley, A.M., Yang, W.S., et al. (2012). Ferroptosis: an iron-dependent form of nonapoptotic cell death. Cell *149*, 1060–1072.

Dixon, S.J., Winter, G.E., Musavi, L.S., Lee, E.D., Snijder, B., Rebsamen, M., Superti-Furga, G., and Stockwell, B.R. (2015). Human haploid cell genetics reveals roles for lipid metabolism genes in nonapoptotic cell death. ACS Chem. Biol. *10*, 1604–1609.

Doll, S., Proneth, B., Tyurina, Y.Y., Panzilius, E., Kobayashi, S., Ingold, I., Irmler, M., Beckers, J., Aichler, M., Walch, A., et al. (2017). ACSL4 dictates ferroptosis sensitivity by shaping cellular lipid composition. Nat. Chem. Biol. *13*, 91–98.

Doll, S., Freitas, F.P., Shah, R., Aldrovandi, M., da Silva, M.C., Ingold, I., Goya Grocin, A., Xavier da Silva, T.N., Panzilius, E., Scheel, C.H., et al. (2019). FSP1 is a glutathione-independent ferroptosis suppressor. Nature *575*, 693–698.

Ducker, G.S., Ghergurovich, J.M., Mainolfi, N., Suri, V., Jeong, S.K., Hsin-Jung Li, S., Friedman, A., Manfredi, M.G., Gitai, Z., Kim, H., and Rabinowitz, J.D. (2017). Human SHMT inhibitors reveal defective glycine import as a targetable metabolic vulnerability of diffuse large B-cell lymphoma. Proc. Natl. Acad. Sci. USA *114*, 11404–11409.

Fan, Z., Wirth, A.K., Chen, D., Wruck, C.J., Rauh, M., Buchfelder, M., and Savaskan, N. (2017). Nrf2-Keap1 pathway promotes cell proliferation and diminishes ferroptosis. Oncogenesis *6*, e371.

Furuyama, K., and Sassa, S. (2000). Interaction between succinyl CoA synthetase and the heme-biosynthetic enzyme ALAS-E is disrupted in sideroblastic anemia. J. Clin. Invest. *105*, 757–764.

Gao, M., Monian, P., Quadri, N., Ramasamy, R., and Jiang, X. (2015). Glutaminolysis and transferrin regulate ferroptosis. Mol. Cell *59*, 298–308.

Gao, M., Yi, J., Zhu, J., Minikes, A.M., Monian, P., Thompson, C.B., and Jiang, X. (2019). Role of mitochondria in ferroptosis. Mol. Cell *73*, 354–363.e3.

Gaschler, M.M., Hu, F., Feng, H., Linkermann, A., Min, W., and Stockwell, B.R. (2018). Determination of the subcellular localization and mechanism of action of ferrostatins in suppressing ferroptosis. ACS Chem. Biol. *13*, 1013–1020.

Greenfeld, H., Takasaki, K., Walsh, M.J., Ersing, I., Bernhardt, K., Ma, Y., Fu, B., Ashbaugh, C.W., Cabo, J., Mollo, S.B., et al. (2015). TRAF1 coordinates polyubiquitin signaling to enhance Epstein-Barr virus LMP1-mediated growth and survival pathway activation. PLoS Pathog. *11*, e1004890.

Habib, E., Linher-Melville, K., Lin, H.-X., and Singh, G. (2015). Expression of xCT and activity of system xc(-) are regulated by NRF2 in human breast cancer cells in response to oxidative stress. Redox Biol. *5*, 33–42.

Hanigan, M.H., and Pitot, H.C. (1985). Gamma-glutamyl transpeptidase–its role in hepatocarcinogenesis. Carcinogenesis *6*, 165–172.

Harris, I.S., and DeNicola, G.M. (2020). The complex interplay between antioxidants and ROS in cancer. Trends Cell Biol. *30*, 440–451.

Harris, I.S., Treloar, A.E., Inoue, S., Sasaki, M., Gorrini, C., Lee, K.C., Yung, K.Y., Brenner, D., Knobbe-Thomsen, C.B., Cox, M.A., et al. (2015). Glutathione and thioredoxin antioxidant pathways synergize to drive cancer initiation and progression. Cancer Cell *27*, 211–222.

Harris, I.S., Endress, J.E., Coloff, J.L., Selfors, L.M., McBrayer, S.K., Rosenbluth, J.M., Takahashi, N., Dhakal, S., Koduri, V., Oser, M.G., et al. (2019). Deubiquitinases maintain protein homeostasis and survival of cancer cells upon glutathione depletion. Cell Metab. *29*, 1166–1181.e6.

Hayes, J.D., and McMahon, M. (2009). NRF2 and KEAP1 mutations: permanent activation of an adaptive response in cancer. Trends Biochem. Sci. *34*, 176–188.

Huang, C.-S., Moore, W.R., and Meister, A. (1988). On the active site thiol of gamma-glutamylcysteine synthetase: relationships to catalysis, inhibition, and regulation. Proc. Natl. Acad. Sci. USA *85*, 2464–2468.

Huang, Z.-Z., Chen, C., Zeng, Z., Yang, H., Oh, J., Chen, L., and Lu, S.C. (2001). Mechanism and significance of increased glutathione level in human hepatocellular carcinoma and liver regeneration. FASEB J. *15*, 19–21.

Ji, X., Qian, J., Rahman, S.M.J., Siska, P.J., Zou, Y., Harris, B.K., Hoeksema, M.D., Trenary, I.A., Heidi, C., Eisenberg, R., et al. (2018). xCT (SLC7A11)-mediated metabolic reprogramming promotes non-small cell lung cancer progression. Oncogene *37*, 5007–5019.

Jiang, L., Kon, N., Li, T., Wang, S.-J., Su, T., Hibshoosh, H., Baer, R., and Gu, W. (2015). Ferroptosis as a p53-mediated activity during tumour suppression. Nature *520*, 57–62.

Kang, Y.P., Torrente, L., Falzone, A., Elkins, C.M., Liu, M., Asara, J.M., Dibble, C.C., and DeNicola, G. (2019). Cysteine dioxygenase 1 is a metabolic liability for non-small cell lung cancer. eLife *8*, e45572.

Kobayashi, S., Ikeda, Y., Shigeno, Y., Konno, H., and Fujii, J. (2020). -Glutamylcysteine synthetase and γ-glutamyl transferase as differential enzymatic sources of γ-glutamylpeptides in mice. Amino Acids *52*, 555–566.

Leu, J.I., Murphy, M.E., and George, D.L. (2019). Mechanistic basis for impaired ferroptosis in cells expressing the African-centric S47 variant of p53. Proc. Natl. Acad. Sci. USA *116*, 8390–8396.

Lim, J.K.M., Delaidelli, A., Minaker, S.W., Zhang, H.-F., Colovic, M., Yang, H., Negri, G.L., von Karstedt, S., Lockwood, W.W., Schaffer, P., et al. (2019). Cystine/glutamate antiporter xCT (SLC7A11) facilitates oncogenic RAS transformation by preserving intracellular redox balance. Proc. Natl. Acad. Sci. USA *116*, 9433–9442.

Mancias, J.D., Wang, X., Gygi, S.P., Harper, J.W., and Kimmelman, A.C. (2014). Quantitative proteomics identifies NCOA4 as the cargo receptor mediating ferritinophagy. Nature *509*, 105–109.

Martínez-Reyes, I., Diebold, L.P., Kong, H., Schieber, M., Huang, H., Hensley, C.T., Mehta, M.M., Wang, T., Santos, J.H., Woychik, R., et al. (2016). TCA cycle and mitochondrial membrane potential are necessary for diverse biological functions. Mol. Cell *61*, 199–209.

Monroe, D.H., and Eaton, D.L. (1988). Effects of modulation of hepatic glutathione on biotransformation and covalent binding of aflatoxin B1 to DNA in the mouse. Toxicol. Appl. Pharmacol. *94*, 118–127.

Ookhtens, M., and Kaplowitz, N. (1998). Role of the liver in interorgan homeostasis of glutathione and cyst(e)ine. Semin. Liver Dis. *18*, 313–329.

Oppenheimer, L., Wellner, V.P., Griffith, O.W., and Meister, A. (1979). Glutathione synthetase. Purification from rat kidney and mapping of the substrate binding sites. J. Biol. Chem. *254*, 5184–5190.

Penno, A., Reilly, M.M., Houlden, H., Laurá, M., Rentsch, K., Niederkofler, V., Stoeckli, E.T., Nicholson, G., Eichler, F., Brown, R.H., Jr., et al. (2010). Hereditary sensory neuropathy type 1 is caused by the accumulation of two neurotoxic sphingolipids. J. Biol. Chem. *285*, 11178–11187.

Poursaitidis, I., Wang, X., Crighton, T., Labuschagne, C., Mason, D., Cramer, S.L., Triplett, K., Roy, R., Pardo, O.E., Seckl, M.J., et al. (2017). Oncogene-selective sensitivity to synchronous cell death following modulation of the amino acid nutrient cystine. Cell Rep. *18*, 2547–2556.

Rao, A.M., Drake, M.R., and Stipanuk, M.H. (1990). Role of the transsulfuration pathway and of gamma-cystathionase activity in the formation of cysteine and sulfate from methionine in rat hepatocytes. J. Nutr. *120*, 837–845.

Reed, D.J., and Orrenius, S. (1977). The role of methionine in glutathione biosynthesis by isolated hepatocytes. Biochem. Biophys. Res. Commun. *77*, 1257–1264.

Richman, P.G., and Meister, A. (1975). Regulation of gamma-glutamylcysteine synthetase by nonallosteric feedback inhibition by glutathione. J. Biol. Chem. *250*, 1422–1426.

Ristoff, E., and Larsson, A. (2007). Inborn errors in the metabolism of glutathione. Orphanet J. Rare Dis. *2*, 16.

Rouault, T.A. (2012). Biogenesis of iron-sulfur clusters in mammalian cells: new insights and relevance to human disease. Dis. Model. Mech. *5*, 155–164.

Sasaki, H., Sato, H., Kuriyama-Matsumura, K., Sato, K., Maebara, K., Wang, H., Tamba, M., Itoh, K., Yamamoto, M., and Bannai, S. (2002). Electrophile response element-mediated induction of the cystine/glutamate exchange transporter gene expression. J. Biol. Chem. *277*, 44765–44771.

Sayin, V.I., LeBoeuf, S.E., Singh, S.X., Davidson, S.M., Biancur, D., Guzelhan, B.S., Alvarez, S.W., Wu, W.L., Karakousi, T.R., Zavitsanou, A.M., et al. (2017). Activation of the NRF2 antioxidant program generates an imbalance in central carbon metabolism in cancer. eLife *6*, e28083.

Shin, C.-S., Mishra, P., Watrous, J.D., Carelli, V., D'Aurelio, M., Jain, M., and Chan, D.C. (2017). The glutamate/cystine xCT antiporter antagonizes glutamine metabolism and reduces nutrient flexibility. Nat. Commun. *8*, 15074.

Sofyanovich, O.A., Nishiuchi, H., Yamagishi, K., Matrosova, E.V., and Serebrianyi, V.A. (2019). Multiple pathways for the formation of the γ-glutamyl peptides γ-glutamyl-valine and γ-glutamyl-valyl-glycine in Saccharomyces cerevisiae. PLoS ONE *14*, e0216622.

Soga, T., Sugimoto, M., Honma, M., Mori, M., Igarashi, K., Kashikura, K., Ikeda, S., Hirayama, A., Yamamoto, T., Yoshida, H., et al. (2011). Serum metabolomics reveals γ-glutamyl dipeptides as biomarkers for discrimination among different forms of liver disease. J. Hepatol. *55*, 896–905.

Soini, Y., Näpänkangas, U., Järvinen, K., Kaarteenaho-Wiik, R., Pääkkö, P., and Kinnula, V.L. (2001). Expression of gamma-glutamyl cysteine synthetase in nonsmall cell lung carcinoma. Cancer *92*, 2911–2919.

Solmonson, A., and DeBerardinis, R.J. (2018). Lipoic acid metabolism and mitochondrial redox regulation. J. Biol. Chem. *293*, 7522–7530.

Soula, M., Weber, R.A., Zilka, O., Alwaseem, H., La, K., Yen, F., Molina, H., Garcia-Bermudez, J., Pratt, D.A., and Birsoy, K. (2020). Metabolic determinants of cancer cell sensitivity to canonical ferroptosis inducers. Nat. Chem. Biol. *16*, 1351–1360.

Stipanuk, M.H., Dominy, J.E., Jr., Lee, J.-I., and Coloso, R.M. (2006). Mammalian cysteine metabolism: new insights into regulation of cysteine metabolism. J. Nutr. *136* (*Suppl*), 1652S–1659S.

Stipanuk, M.H., Ueki, I., Dominy, J.E., Jr., Simmons, C.R., and Hirschberger, L.L. (2009). Cysteine dioxygenase: a robust system for regulation of cellular cysteine levels. Amino Acids *37*, 55–63.

Sun, X., Ou, Z., Chen, R., Niu, X., Chen, D., Kang, R., and Tang, D. (2016). Activation of the p62-Keap1-NRF2 pathway protects against ferroptosis in hepatocellular carcinoma cells. Hepatology *63*, 173–184.

Sun, J., Zhou, C., Ma, Q., Chen, W., Atyah, M., Yin, Y., Fu, P., Liu, S., Hu, B., Ren, N., and Zhou, H. (2019). High GCLC level in tumor tissues is associated with poor prognosis of hepatocellular carcinoma after curative resection. J. Cancer *10*, 3333–3343.

Takeuchi, S., Wada, K., Toyooka, T., Shinomiya, N., Shimazaki, H., Nakanishi, K., Nagatani, K., Otani, N., Osada, H., Uozumi, Y., et al. (2013). Increased xCT expression correlates with tumor invasion and outcome in patients with glioblastomas. Neurosurgery *72*, 33–41, discussion 41.

Tatebe, S., Unate, H., Sinicrope, F.A., Sakatani, T., Sugamura, K., Makino, M., Ito, H., Savaraj, N., Kaibara, N., and Kuo, M.T. (2002). Expression of heavy subunit of gamma-glutamylcysteine synthetase (gamma-GCSh) in human colorectal carcinoma. Int. J. Cancer *97*, 21–27.

Timmerman, L.A., Holton, T., Yuneva, M., Louie, R.J., Padró, M., Daemen, A., Hu, M., Chan, D.A., Ethier, S.P., van 't Veer, L.J., et al. (2013). Glutamine sensitivity analysis identifies the xCT antiporter as a common triple-negative breast tumor therapeutic target. Cancer Cell *24*, 450–465.

Torrente, L., Sanchez, C., Moreno, R., Chowdhry, S., Cabello, P., Isono, K., Koseki, H., Honda, T., Hayes, J.D., Dinkova-Kostova, A.T., and de la Vega, L. (2017). Crosstalk between NRF2 and HIPK2 shapes cytoprotective responses. Oncogene *36*, 6204–6212.

Ventura, A., Kirsch, D.G., McLaughlin, M.E., Tuveson, D.A., Grimm, J., Lintault, L., Newman, J., Reczek, E.E., Weissleder, R., and Jacks, T. (2007). Restoration of p53 function leads to tumour regression in vivo. Nature *445*, 661–665.

Vyas, S., Zaganjor, E., and Haigis, M.C. (2016). Mitochondria and cancer. Cell *166*, 555–566.

Weinstein, C.L., Haschemeyer, R.H., and Griffith, O.W. (1988). In vivo studies of cysteine metabolism. Use of D-cysteinesulfinate, a novel cysteinesulfinate decarboxylase inhibitor, to probe taurine and pyruvate synthesis. J. Biol. Chem. *263*, 16568–16579.

Winterbourn, C.C., and Hampton, M.B. (2008). Thiol chemistry and specificity in redox signaling. Free Radic. Biol. Med. *45*, 549–561.

Yang, W.S., SriRamaratnam, R., Welsch, M.E., Shimada, K., Skouta, R., Viswanathan, V.S., Cheah, J.H., Clemons, P.A., Shamji, A.F., Clish, C.B., et al. (2014). Regulation of ferroptotic cancer cell death by GPX4. Cell *156*, 317–331.

Zhang, Y., Tan, H., Daniels, J.D., Zandkarimi, F., Liu, H., Brown, L.M., Uchida, K., O'Connor, O.A., and Stockwell, B.R. (2019). Imidazole ketone erastin induces ferroptosis and slows tumor growth in a mouse lymphoma model. Cell Chem. Biol. *26*, 623–633.e9.

Zhang, T., Bauer, C., Newman, A.C., Uribe, A.H., Athineos, D., Blyth, K., and Maddocks, O.D.K. (2020). Polyamine pathway activity promotes cysteine essentiality in cancer cells. Nat Metab *2*, 1062–1076.

Zou, Y., and Schreiber, S.L. (2020). Progress in understanding ferroptosis and challenges in its targeting for therapeutic benefit. Cell Chem. Biol. *27*, 463–471.

Please cite this article in press as: Kang et al., Non-canonical Glutamate-Cysteine Ligase Activity Protects against Ferroptosis, Cell Metabolism (2020), https://doi.org/10.1016/j.cmet.2020.12.007

STAR★METHODS

KEY RESOURCES TABLE

REAGENT or RESOURCE	SOURCE	IDENTIFIER
Antibodies		
GCLC (Mouse monoclonal Ab)	Santa Cruz Biotechnology	Cat#: sc-390811; Lot#: E1917; RRID: AB_2736837
GSS (Mouse monoclonal Ab)	Novus Biologicals	Cat#: NBP2-03351; Lot#: A01
GCLM (Rabbit polyclonal Ab)	GeneTex	Cat#: GTX114075; Lot#: 40156; RRID: AB_10619535
GPX4 (Mouse monoclonal Ab)	R&D Systems	Cat#: MAB5457; Lot#: CCXW0218061; RRID: AB_2232542
β-Actin (Mouse monoclonal Ab)	Thermo Fisher Scientific	Cat#: AM4302; Lot#: 00867595; RRID: AB_2536382
xCT (Rabbit polyclonal Ab)	Abcam	Cat#: ab37185; Lot#: GR3275067-8; RRID: AB_778944
HSP90 (Rabbit polyclonal Ab)	Cell Signaling Technology	Cat#: 4874S; Lot# 5; RRID: AB_2121214
Chemicals, Peptides, and Recombinant Proteins		
Sytox Green	Thermo Fisher Scientific	Cat#: S7020
Cytotox Red	Thermo Fisher Scientific	Cat#: NC1015259
DMSO	VWR Scientific Inc	Cat#: 97063-136
0.4% PFA in PBS	Thermo Fisher Scientific	Cat#: J19943-K2
Tamoxifen	Sigma-Aldrich	Cat#: T5648-5G
Arginine	Sigma-Aldrich	Cat#:A6969-25G
Aspartate	MP Biomedicals	Cat#:219463380
Asparagine	Sigma-Aldrich	Cat#:A4159-25G
Glutamate	Sigma-Aldrich	Cat#:G8415-100G
Glutamine	VWR	Cat#:VWRL0131-0100
Glycine	VWR	Cat#:BP381-1
Histidine	Sigma-Aldrich	Cat#:H5659-25G
Hydroxy-L-proline	VWR	Cat#:TCH0296-5G
Isoleucine	VWR	Cat#:AAJ63045-14
Leucine	Sigma-Aldrich	Cat#:L8912-25G
Lysine	Sigma-Aldrich	Cat#:L8662-25G
Methionine	Sigma-Aldrich	Cat#:M5308-25G
Phenylalanine	Sigma-Aldrich	Cat#:P5482-25G
Proline	Sigma-Aldrich	Cat#:P5607-25G
Threonine	VWR	Cat#:97064-026
Tryptophan	Sigma-Aldrich	Cat#:T8941-25G
Tyrosine	Sigma-Aldrich	Cat#:T1145-25G
Valine	Sigma-Aldrich	Cat#:V0513-25G
Glucose	Sigma-Aldrich	Cat#:G7021-100G
$[^{2}H_{5}]$-GSH	Santa Cruz Biotechnology	Cat#: sc-489493
$[^{13}C_{3}, ^{15}N]$-cysteine	Cambridge Isotope Laboratories	Cat#: CNLM-3871-H-0.25

(*Continued on next page*)

Please cite this article in press as: Kang et al., Non-canonical Glutamate-Cysteine Ligase Activity Protects against Ferroptosis, Cell Metabolism (2020), https://doi.org/10.1016/j.cmet.2020.12.007

Continued

REAGENT or RESOURCE	SOURCE	IDENTIFIER
[2, 3, 3-$^{2}H_3$]-serine	Cambridge Isotope Laboratories	Cat#: DLM-582- 0.1
[$^{13}C_3$]-serine	Cambridge Isotope Laboratories	Cat#: CLM-1574-H-0.1
[$^{13}C_5$, $^{15}N_2$]-glutamine	Cambridge Isotope Laboratories	Cat#: CNLM-1275-H-0.1
METABOLOMICS AMINO ACID MIX STANDARD	Cambridge Isotope Laboratories	Cat#: MSK-A2-1.2
γ-glutamyl-alanine	Santa Cruz Biotechnology	Cat#: sc-300878
γ-glutamyl-glycine	Bachem	Cat#: 4003498.0001
γ-glutamyl-leucine	Bachem	Cat#: 4005004.0001
γ-glutamyl-valine	Bachem	Cat#: 4003707.0250
MeOH (HPLC grade)	Sigma Aldrich	Cat#: 34860-1 L-R
H_2O (HPLC grade)	Fisher Chemical	Cat#: W5-1
Acetonitrile (HPLC grade)	Honeywell	Cat#: 34967
N-ethylmaleimide (NEM)	Alfa Aesar	Cat#: 40526-06
Blasticidin	Invivogen	Cat#: ant-bl-1
Puromycin	Invivogen	Cat#: ant-pr-1
Hygromycin	Invivogen	Cat#: ant-hg-1
Glutamate diethyl ester (GluEE)	TCI Chemicals	Cat#: G0179-5G
Cystine	Sigma Aldrich	Cat#: C6727-25G
Erastin	Cayman Chemical	Cat#: 17754
Ferrostatin-1 (Fer-1)	Cayman Chemical	Cat#: 17729
Deferoxamine (DFO)	Sigma Aldrich	Cat#: D9533-1G
AOA	Santa Cruz Biotechnology	Cat#: sc-207410
SHIN-1	Dr. Joshua Rabinowitz, Department of Chemistry and Lewis-Sigler Institute for Integrative Genomics (Princeton University)	(Ducker et al., 2017)
L-Buthionine-(S,R)-Sulfoximine (BSO)	Cayman Chemical or Sigma Aldrich	Cat#: 14484 or Cat#: B2515-500MG
Cyst(e)inase	Dr. Everett Stone, Department of Molecular Biosciences (University of Texas Austin)	(Cramer et al., 2017)
KI-696	MedChem Express	Cat#: HY-101140
2755 Glutamate Standard	YSI	Cat#: 027055
Critical Commercial Assays		
CellROX green	Fisher Scientific	Cat#: C10444
BODIPY-C11	Invitrogen	Cat#: C10445
MitoSOX Red	Invitrogen	Cat#: M36008
Experimental Models: Cell Lines		
PC9	Dr John Minna, Hamon Cancer Center Collection (University of Texas-Southwestern Medical Center)	RRID: CVCL_B260
H810	Dr John Minna, Hamon Cancer Center Collection (University of Texas-Southwestern Medical Center)	RRID: CVCL_1590
H2172	Dr John Minna, Hamon Cancer Center Collection (University of Texas-Southwestern Medical Center)	RRID: CVCL_1537
Calu3	Dr John Minna, Hamon Cancer Center Collection (University of Texas-Southwestern Medical Center)	RRID: CVCL_0609
H1581	Dr John Minna, Hamon Cancer Center Collection (University of Texas-Southwestern Medical Center)	RRID: CVCL_1479

(*Continued on next page*)

Please cite this article in press as: Kang et al., Non-canonical Glutamate-Cysteine Ligase Activity Protects against Ferroptosis, Cell Metabolism (2020), https://doi.org/10.1016/j.cmet.2020.12.007

Continued

REAGENT or RESOURCE	SOURCE	IDENTIFIER
H1975	Dr John Minna, Hamon Cancer Center Collection (University of Texas-Southwestern Medical Center)	RRID: CVCL_1511
H2087	Dr John Minna, Hamon Cancer Center Collection (University of Texas-Southwestern Medical Center)	RRID: CVCL_1524
H2347	Dr John Minna, Hamon Cancer Center Collection (University of Texas-Southwestern Medical Center)	RRID: CVCL_1550
H1792	Dr John Minna, Hamon Cancer Center Collection (University of Texas-Southwestern Medical Center)	RRID: CVCL_1495
H1944	Dr John Minna, Hamon Cancer Center Collection (University of Texas-Southwestern Medical Center)	RRID: CVCL_1508
H460	Dr John Minna, Hamon Cancer Center Collection (University of Texas-Southwestern Medical Center)	RRID: CVCL_0459
HCC15	Dr John Minna, Hamon Cancer Center Collection (University of Texas-Southwestern Medical Center)	RRID: CVCL_2057
H2009	ATCC	Cat#: CRL-5911; RRID: CVCL_1514
H1299	ATCC	Cat#: CRL-5803; RRID: CVCL_0060
H1993	ATCC	Cat#: CRL-5909; RRID: CVCL_1512
H441	ATCC	Cat#: HTB-174; RRID: CVCL_1561
A549	ATCC	Cat#: CCL-185; RRID: CVCL_0023
NRF2 KO A549	Dr. Laureano de la Vega	(Torrente et al., 2017)
Lenti-X 293T	Clontech	Cat#: 632180
Experimental Models: Organisms/Strains		
Gclc$^{f/f}$	(Chen et al., 2007)	N/A
R26-CreERT2	(Ventura et al., 2007)	N/A
Oligonucleotides		
Guide RNA for lentiCRISPR-V2 GCLC; Forward: 5′-caccgTAGATGTGCAGGAACTGG-3′; Reverse: 5′-aaacCCAGTTCCTGCACATCTAc-3′	(Harris et al., 2019)	N/A
Guide RNA for lentiCRISPR-V2 GSS; Forward: 5′-caccgGGTCTCTGGACCAAGACCGA-3′; Reverse: 5′-aaacTCGGTCTTGGTCCAGAGACc-3′	This study	N/A
PCR primer for pLenti-hygromycin-GCLC; Forward: 5′-cgactctagaggatccatggggctgctgtcc-3′; Reverse: 5′-gaggttgattgtcgacctagttggatgagtcagttttacttcc-3′	This study	N/A
PCR primer for pLenti-hygromycin-GSS; Forward: 5′-cgactctagaggatccatggccaccaactgg-3′; Reverse: 5′-gaggttgattgtcgactcacacagggtatgggttgtc-3′	This study	N/A
Site directed mutagenesis primer for pLenti-hygromycin-$GCLC_{Res}$; Forward: 5′- GGCACGGGATTCTCCAGTTCCTG −3′; Reverse: 5′- GCCGCACGTGGTCGGCAT −3′	This study	N/A
Site directed mutagenesis primer for pLenti-hygromycin-GSS_{Res}; Forward: 5′- AAGACCGAAGACTGTTTGTGG −3′; Reverse: 5′- GGTCCAGAGACCCCTTTT-3′	This study	N/A

(*Continued on next page*)

Please cite this article in press as: Kang et al., Non-canonical Glutamate-Cysteine Ligase Activity Protects against Ferroptosis, Cell Metabolism (2020), https://doi.org/10.1016/j.cmet.2020.12.007

Continued

REAGENT or RESOURCE	SOURCE	IDENTIFIER
Recombinant DNA		
lentiCas9-Blast	Addgene	Cat#: 52962
lentiCRISPR-V2	Addgene	Cat#: 52961
lentiCRISPR-V2 GCLC; Using BsmBI restriction site, primers were annealed and cloned to progenitor of lentiCRISPR-V2.	This study	N/A
lentiCRISPR-V2 GSS; Using BsmBI restriction site, primers were annealed and cloned to progenitor of lentiCRISPR-V2	This study	N/A
MGC Human GCLC Sequence-Verified cDNA (pCMV-SPORT6-GCLC)	Dharmacon	Cat#: MHS6278-202759380
MGC Human GSS Sequence-Verified cDNA (pOTB7-GSS)	Dharmacon	Cat#: MHS6278-202830404
pLenti-hygro-GFP	Addgene	Cat#: 17446
pLenti-hygro-GCLC resistant to sgGCLC (pLH-GCLC$_{Res}$); The GFP of pLenti-hygro-GFP was excised and replaced with human GCLC cDNA using MGC Human GCLC Sequence-Verified cDNA (pCMV-SPORT6-GCLC) as a PCR template. The pLenti-hygro-GCLC resistant to sgGCLC was further generated by the site-directed mutagenesis.	This study	N/A
pLenti-hygro-GSS resistant to sgGSS (pLH-GSS$_{Res}$); The GFP of pLenti-hygro-GFP was excised and replaced with human GSS cDNA using MGC Human GSS Sequence-Verified cDNA (pOTB7-GSS) as a PCR template. The pLenti-hygro-GSS resistant to sgGSS was further generated by the site-directed mutagenesis.	This study	N/A
pCMV-dR8.2 dvpr	Addgene	Cat#: 8455
pCMV-VSV-G	Addgene	Cat#: 8454
Software and Algorithms		
EL-Maven	https://resources.elucidata.io/elmaven	Version 0.6.1, 0.10.0, or 0.11.0
GraphPad Prism	https://www.graphpad.com/scientific-software/prism/	Version 8
IncuCyte Zoom	Essen BioScience	IncuCyte Zoom 2018A
IncuCyte S3	Essen BioScience	IncuCyte S3 2018B or 2020A
Accuri	BD Biosciences	Version C6
FlowJo	BD Biosciences	Version 10.7.1
Other		
RPMI 1640 Medium Modified w/o L-Glutamine, w/o Amino acids, Glucose (Powder)	US Biological	Cat# R9010-01
cysteine/cystine/glutamine/methionine free RPMI	MP Biomedicals	Cat# 091646454
Dialyzed FBS (dFBS)	Sigma Aldrich	Cat# F0392

RESOURCE AVAILABILITY

Lead Contact

Further information and requests for resources and reagents should be directed to and will be fulfilled by the Lead Contact, Dr. Gina M. DeNicola (Gina.DeNicola@moffitt.org).

Material Availability

All unique reagents generated in this study are available from the Lead Contact without restriction.

Data and Code Availability

This study did not generate any unique datasets or code.

Please cite this article in press as: Kang et al., Non-canonical Glutamate-Cysteine Ligase Activity Protects against Ferroptosis, Cell Metabolism (2020), https://doi.org/10.1016/j.cmet.2020.12.007

EXPERIMENTAL MODEL AND SUBJECT DETAILS

Animal Experiments

All animal studies with *Gclc*$^{f/f}$ mice were performed according to protocols approved by the Institutional Animal Care and Use Committee, the Standing Committee on Animals at Harvard University. Mice were housed under standard housing conditions. *Gclc*$^{f/f}$ (Chen et al., 2007) and *R26-CreERT2* (Ventura et al., 2007) mice were bred to generate *Gclc*$^{f/f}$; *R26-CreERT2* mice (C57BL/6 background). *Gclc*$^{f/f}$ (Gclc WT) and *Gclc*$^{f/f}$; *R26-CreERT2* (Gclc KO) adult male and female mice (aged 11-17 weeks old) were treated with tamoxifen (20 mg/mL; dissolved in corn oil) via daily intraperitoneal injection for 5 consecutive days at 160 mg/kg (tamoxifen/mouse body mass). At 14-16 days following the last tamoxifen injection, blood was collected via the retro-orbital venous sinus into BD Microtainer serum separator tubes (catalog #365967) and placed on ice. Mice were euthanized (isoflurane inhalation followed by cervical dislocation) and the liver, kidney, and lung were immediately harvested and small tissue pieces were snap frozen in dry ice. Serum was isolated by centrifugation (16 min at 3000 g) and serum aliquots were snap frozen on dry ice. Tissues and serum were stored at −80°C prior to analysis. All studies with cyst(e)inase/BSO experiments were approved by and conducted in accordance to the ethical standards established by the University of South Florida IACUC (protocol # R IS00007922). Mice were housed under standard housing conditions. For cyst(e)inase/BSO experiments, C57BL/6J female mice (aged 7 weeks old) were treated with Cyst(e)inase (75 mg/kg) or vehicle (PBS) via intraperitoneal injection. After 24 h, the mice were further treated with BSO (10 mmol/kg) prepared as previously described (Monroe and Eaton, 1988) or vehicle (saline) via intraperitoneal injection. After 4 h, blood was collected from the submandibular vein into BD Microtainer serum separator tubes and placed on ice. Mice were then euthanized by cervical dislocation and the liver, kidney, and lung were immediately harvested and small pieces snap frozen in liquid nitrogen. Serum was isolated by centrifugation (16 min at 3000 g) and serum aliquots were snap frozen on dry ice. Tissues and serum were stored at −80°C prior to analysis.

METHOD DETAILS

Lentivirus Generation

Lentiviruses were generated by overnight PEI transfection of 90% confluent Lenti-X 293T cells (Clontech) with target lentiviral plasmid, and packaging plasmids pCMV-dR8.2 dvpr and pCMV-VSV-G in DMEM (10% FBS). The next day, the medium was changed to fresh DMEM (10% FBS). After 24 and 48 h, the virus containing medium was collected and filtered with a 0.45 μm PES filter. The two collections were combined and stored at −80°C until virus infection.

Lentiviral Infection of NSCLC Cells

To increase gene deletion efficiency in a polyclonal population, H1299 cells with stable *Streptococcus pyogenes* Cas9 expression (H1299^{Cas9}) were first established by lentiviral transduction with lentiCas9-Blast (Greenfeld et al., 2015) followed by blasticidin selection (3 mg/mL) for 5 days. To generate GCLC or GSS KO cells, H1299^{Cas9} and A549 cells were transduced with empty pLenti-CRISPR-V2 or pLenti-CRISPR-V2 encoding sgGCLC or sgGSS with 2 μg/mL of polybrene, followed by puromycin selection (1 μg/mL) for 4 days. To select single clones for GCLC or GSS KO, transduced A549 cells were diluted to 0.5 cells/well in 96 well dishes in RPMI supplemented with 1 μM of Fer-1. Cells were grown for 2 weeks, followed by expansion of clones. GCLC or GSS KO was verified by loss of GCLC or GSS protein via immunoblotting. Subsequently, cells were reconstituted with sgRNA-resistant cDNAs by transduction with pLenti-hygro-GFP, pLenti-hygro-sgRNA-resistant GCLC (pLH-GCLC$_{Res}$), or pLenti-hygro-sgRNA-resistant GSS (pLH-GSS$_{Res}$) followed by hygromycin selection (300 μg/mL) for 5 days. NRF2 KO A549 cells were reconstituted with NRF2 or empty vector as described previously (Kang et al., 2019).

Dead Cell Measurement with IncuCyte

Cells were plated in black walled 96 well pates at a density of 10,000 cells/well in 100 μL final volume. The next day, the medium was changed to 100 μL of experimental medium containing 20 nM of Sytox Green or 250 nM Cytotox Red as follows: In cystine starvation experiments, cysteine/cystine, methionine and glutamine free RPMI (MP Biomedicals) was supplemented with 100 μM methionine and 10% dialyzed FBS (dFBS) containing 2 mM glutamine with or without 200 μM cystine as indicated. In experiments additionally lacking glutamine and/or glutamate, RPMI 1640 Medium without glucose and amino acids (US Biological) was prepared from powder according the manufacturer's instructions and supplemented with glucose and amino acids to meet the RPMI formulation with the exception of cystine, glutamine, and glutamate. This media was further supplemented with 200 μM of cystine, 2 mM of glutamine, and/or 137 μM of glutamate as indicated. In addition, 10 μM Ferrostatin-1 (Fer-1), 100 μM DFO, 5 mM of GluEE, 0.5 mM AOA, 5 μM Erastin, 0.0625-2 mM γ-glutamyl-dipeptides, and/or 100 μM BSO were added as indicated. The number of dead cells and cell confluence were measured by the IncuCyte Zoom or S3 live-cell analysis system (Essen BioScience, Ann Arbor, MI, USA) in a humidified tissue culture incubator at 37°C with 5% CO_2. Data were acquired with a 4X or 10X objective lens in phase contrast and green fluorescence (Ex/Em: 460/524 nm, acquisition time: 400 ms) or red fluorescence (Ex/Em: 585/635 nm, acquisition time: 300 ms) channels. Images were acquired from each well at 2-4 h intervals. Image and data processing were performed with IncuCyte Zoom 2018A, S3 2018B, or 2020A software (Essen BioScience, Ann Arbor, MI, USA). Dead cell number was normalized to cell confluence [Number of Sytox Green or Cytotox Red positive cells/mm^2/cell confluence (% of total image)]. The area under the curve (AUC) was calculated as the sum of the dead cell numbers at each time point.

Please cite this article in press as: Kang et al., Non-canonical Glutamate-Cysteine Ligase Activity Protects against Ferroptosis, Cell Metabolism (2020), https://doi.org/10.1016/j.cmet.2020.12.007

Metabolomics Sample Preparation

For the tissue targeted metabolomics, the frozen liver, lung, and kidney tissue samples were pulverized using a pre-chilled Bio-Pulverizer (59012MS, BioSpec), weighed frozen, and then placed on dry ice. The tissue metabolites were extracted in 80% MeOH at a final tissue concentration of 50 mg/mL for 24 h at −80°C. After centrifugation (17000 g, 20 min, 4°C), the supernatant was analyzed by LC-HRMS.

For the quantitative intracellular $^{13}C_3$-serine tracing and cysteine quantification, NSCLC cells were plated in 6 well dishes and pre-conditioned in RPMI medium containing dFBS (10%) overnight. For serine tracing, RPMI 1640 Medium without glucose and amino acids (US Biological) was prepared from powder according the manufacturer's instructions and supplemented with glucose and amino acids to meet the RPMI formulation with the exception of serine and cystine. The following day, the cells were quickly washed with 1 mL of warm serine/cystine-free RPMI medium, followed by feeding with $^{13}C_3$-serine containing medium (serine/cystine-free RPMI + 10% dFBS + 1% Pen/Strep + 300 μM $^{13}C_3$-Serine) lacking or supplemented with 200 μM cystine. After 4 h, the medium was aspirated and the cells were quickly washed with ice cold PBS. As described in our previous study (Kang et al., 2019), the cellular metabolites were extracted and derivatized with 0.5 mL of ice-cold extraction solvent (80% MeOH:20% H2O containing 25 mM NEM and 10 mM ammonium formate, pH 7.0). The concentration of internal standards in the extraction solvent were as follows: 4.18 μM [$^2H_5$]-GSH-NEM, 2.49 μM [$^{13}C_3$, ^{15}N]-serine, 2.48 μM [$^{13}C_2$, ^{15}N]-glycine, and 2.49 μM [$^{13}C_5$, ^{15}N]-glutamate from METABOLOMICS AMINO ACID MIX STANDARD (Cambridge Isotope Laboratories). For cysteine quantification, the extraction solvent contained 10 μM [$^{13}C_2$, ^{15}N]-cysteine-NEM. [$^2H_5$]-GSH-NEM and [$^{13}C_2$, ^{15}N]-cysteine-NEM were pre-prepared by reaction of 50 mM NEM (10 mM ammonium formate, pH 7.0) for 30 min as previously described (Kang et al., 2019). After incubation on ice for 30 min, the NEM-derivatized metabolite extracts were cleared by centrifugation and the supernatant was analyzed by LC-HRMS at the positive mode. For metabolite concentration calculations, the total volume of the cell pellet from a duplicate well was used to calculate the intracellular metabolite concentrations. Cell volume was determined with a Scepter 2.0 cell counter (Millipore), and cell numbers were determined using either the Scepter 2.0 cell counter or a Beckman coulter cell counter (Z1 S). Total volume of the cell pellet was used to calculate the intracellular metabolite concentrations.

For the intracellular 2, 3, 3- $^2H_3$-serine tracing, A549 cells were prepared as described for $^{13}C_3$-serine tracing but medium containing 300 μM [2, 3, 3-$^2H_3$-serine]-was used. Further, 0.5 μM of SHIN-1 (Ducker et al., 2017) was included in the cystine starved conditions. After 12 h, the medium was aspirated, and cells were quickly washed with ice cold PBS, and cellular metabolites were extracted with 0.5 mL of 80% MeOH (−80°C, 15 min). After scraping, the metabolite extract was transferred into an Eppendorf tube and cleared by centrifugation (17000 g, 20 min, 4°C), followed by LC-HRMS analysis in negative mode.

For the intracellular $^{13}C_5$, $^{15}N_2$-glutamine tracing, A549 cells were plated in 6 well dishes and pre-conditioned in RPMI medium containing dFBS (10%) overnight. Cysteine/cystine, methionine and glutamine free RPMI (MP Biomedicals) was supplemented with 100 μM methionine and 10% dialyzed FBS (dFBS) containing 2 mM $^{13}C_5$, $^{15}N_2$-glutamine with or without 200 μM cystine as indicated. The following day, the cells were quickly washed with 1 mL of warm glutamine/cystine-free RPMI medium, followed by feeding with $^{13}C_5$, $^{15}N_2$-glutamine containing medium lacking or supplemented with 200 μM cystine. After 4 h, the medium was aspirated and the cells were quickly washed with ice cold PBS, and cellular metabolites were extracted with 0.5 mL of 80% MeOH (−80°C, 15 min). After scraping, the metabolite extract was transferred into an Eppendorf tube and cleared by centrifugation (17000 g, 20 min, 4°C), followed by LC-HRMS analysis in negative mode.

For the intracellular non-targeted metabolomics, and Glycine and Glutamate quantification, NSCLC cells were plated in 6 well dishes so they were 70% confluent at the time of extraction and pre-conditioned in RPMI medium containing dFBS (10%) overnight. The following day, the medium was aspirated and the cells were quickly washed with 1 mL of cystine free RPMI (10% dFBS, 1% P/S), followed by feeding with conditioning medium as indicated. 1 mL of the medium supernatant was collected to assay glutamate as indicated. For the non-targeted metabolomics approach, medium was aspirated and cells were quickly washed with ice cold PBS, followed by extraction of cellular metabolites with 0.5 mL of 80% MeOH (−80°C, 15 min). For intracellular glutamate, glycine, alanine, valine, threonine, and leucine quantification, the extraction solvent also contained 2.49 μM of [$^{13}C_5$, ^{15}N]-glutamate, 2.48 μM of [$^{13}C_2$, ^{15}N]-glycine, 2.48 μM of [$^{13}C_3$, ^{15}N]-alanine, 2.49 μM of [$^{13}C_5$, ^{15}N]-valine, 2.45 μM of [$^{13}C_4$, ^{15}N]-threonine, and 2.48 μM of [$^{13}C_6$, ^{15}N]-leucine from METABOLOMICS AMINO ACID MIX STANDARD (Cambridge Isotope Laboratories). After scraping, the metabolite extract was transferred into an Eppendorf tube and cleared by centrifugation (17000 g, 20 min, 4°C), followed by LC-HRMS analysis in the negative and/or positive mode. For metabolite concentration calculations, the total volume of the cell pellet from a duplicate well was used to calculate the intracellular metabolite concentrations. Cell volume was determined with a Scepter 2.0 cell counter (Millipore), and cell numbers were determined using either the Scepter 2.0 cell counter or a Beckman coulter cell counter (Z1 S).

Quantitation of Glutamate Exportation

The extracellular medium collected above was transferred to the 96 well plates and glutamate concentrations were measured with an YSI 2900 (Yellow springs, OH, USA) using the 2755 glutamate standard (5 mM). The extracellular glutamate secretion rate (nmol/μL of cell volume/h) was determined from cell volume measurements as described above.

LC-MS Analysis

The LC-MS conditions were identical to previously established methods (Kang et al., 2019). For the chromatographic metabolite separation, the Vanquish UPLC systems were coupled to a Q Exactive HF (QE-HF) mass spectrometer equipped with HESI (Thermo Fisher Scientific, Waltham, MA). The column was a SeQuant ZIC-pHILIC LC column, 5 μm, 150 × 4.6 mm (MilliporeSigma, Burlington,

Please cite this article in press as: Kang et al., Non-canonical Glutamate-Cysteine Ligase Activity Protects against Ferroptosis, Cell Metabolism (2020), https://doi.org/10.1016/j.cmet.2020.12.007

MA) with a SeQuant ZIC-pHILIC guard column, 20 × 4.6 mm (MilliporeSigma, Burlington, MA). Mobile phase A was 10 mM $(NH_4)_2CO_3$ and 0.05% NH_4OH in H2O while mobile phase B was 100% ACN. The column chamber temperature was set to 30°C. The mobile phase condition was set according to the following gradient: 0-13min: 80% to 20% of mobile phase B, 13-15min: 20% of mobile phase B. The ESI ionization mode was positive or negative. The MS scan range (m/z) was set to 60-900. The mass resolution was 120,000 and the AGC target was 3×10^6. The capillary voltage and capillary temperature were set to 3.5 KV and 320°C, respectively. 5 μL of sample was loaded. For targeted metabolomics, the LC-MS peaks were manually identified and integrated by EL-Maven (Version 0.6.1, 0.10.0, or 0.11.0) by matching with a previously established in-house library (Kang et al., 2019). The peak areas of target metabolites were further normalized by the median value of identified metabolite peak areas or the peak area of stable isotope labeled internal standards for further quantification as previously described (Bennett et al., 2008). For the non-targeted metabolomics approach, the LC-MS peaks were automatically extracted and aligned using the Automated Feature Detection function of EL-Maven. After the normalization with the median value of the intensities of LC-MS peaks, the statistical analysis was conducted. The γ-glutamyl-peptide peaks were putatively identified by matching their m/z value with the online HMDB database (http://www.hmdb.ca), and further confirmed by matching the m/z value and retention time of authentic standards. The standards for γ-glutamyl-threonine and γ-glutamyl-alanyl-glycine were not available and were instead validated by stable isotope labeled metabolite tracing (Figures 2C and S2A), as described in the results. The γ-glutamyl-peptide levels relative to the average of γ-glutamyl-peptide levels in cystine starved A549 cells were used to compare γ-glutamyl-peptide levels across panel of NSCLC cell lines.

ROS and Lipid Peroxidation Measurements

NSCLC cells were plated in 24 well dishes at 70,000 cells/well and pre-conditioned in RPMI medium containing dFBS (10%) overnight. The following day, the medium was aspirated, and the cells were quickly washed with warm PBS followed by feeding with the indicated medium conditions. For intracellular ROS measurements, CellROX green was added to the cells at a final concentration of 5 μM for the final 30 min of the experiment. Cells were washed with PBS, detached with trypsin, and transferred to Eppendorf tubes. Following centrifugation (10sec, 17,000 g), the supernatant was aspirated, and the pellet was washed with FACS buffer (PBS containing 0.5% BSA, 2 mM EDTA, 1% P/S, and 25 mM HEPES), and fixed with 4% Paraformaldehyde (PFA) in PBS for 10 min. Following centrifugation (10 s, 17,000 g), the pellet was further washed with FACS buffer, re-suspended to 500 μL of FACS buffer, and filtered into FACS tubes. For mitochondrial superoxide measurements, MitoSOX Red was added to the cells at a final centration of 5 μM for the final 10 min of the experiment. For lipid peroxidation measurements, C11-BODIPY was added to the cells at a final concentration of 10 μM for the final 30 min of the experiment. For both MitoSOX and C11-BODIPY, cells were processed as described for CellROX green, except no fixation with PFA was performed. The samples were analyzed by Accuri C6 flow cytometer (BD biosciences) or BD LSR II flow cytometer (BD Biosciences) using the FITC (CellROX, C11-BODIPY) or PE (MitoSOX) filters. The mean fluorescence intensity (MFI) or median fluorescence intensity (Median FI) were analyzed with the Accuri C6 (BD biosciences) or FlowJo (Ver 10.7.1) software, and further normalized by the control of experimental set as indicated.

Immunoblotting

Cell lysates were prepared in RIPA buffer (20 mM Tris-HCl, pH7.5; 150 mM NaCl, 1 mM EDTA, 1 mM EGTA, 1% NP-40, 1% sodium deoxycholate) containing protease inhibitors. After protein quantification with the Bio-Rad DC assay, the samples were mixed with reducing buffer (v/v, 5:1) containing 2-mercaptoethanol. The proteins were separated by SDS-PAGE using NuPAGE 4%–12% Bis-Tris gels (Invitrogen) and transferred to 0.45 μm Nitrocellulose membrane (GE Healthcare). The membrane was blocked in blocking buffer (5% non-fat milk in TBST) for 15 min, and the membrane was incubated with primary antibodies overnight at the following dilutions: GCLC (1:1000), GCLM (1:1,000), GSS (1:2,000), xCT (1:1,000), GPX4 (1:1,000) β-Actin (1:100,000), HSP90 (1:5,000). After washing the membrane 3 times with TBST for 10 min, the membrane was incubated with secondary antibody (goat anti-rabbit or goat anti-mouse, 1:10,000 dilution, Jackson ImmunoResearch) in blocking buffer for 1 h. After washing the membrane in TBST 3 times for 10 min, the enhanced chemo-luminescence signal was measured by exposing to X-ray film.

QUANTIFICATION AND STATISTICAL ANALYSIS

Statistical analyses were conducted with Graph Pad Prism 8. For the comparison of two groups, two-tailed Student's t test was used. For the comparison of more than 3 experimental groups, one-way ANOVA was used with Bonferroni's multiple comparison test.

Cell Metabolism, Volume *33*

Supplemental Information

Non-canonical Glutamate-Cysteine Ligase Activity Protects against Ferroptosis

Yun Pyo Kang, Andrea Mockabee-Macias, Chang Jiang, Aimee Falzone, Nicolas Prieto-Farigua, Everett Stone, Isaac S. Harris, and Gina M. DeNicola

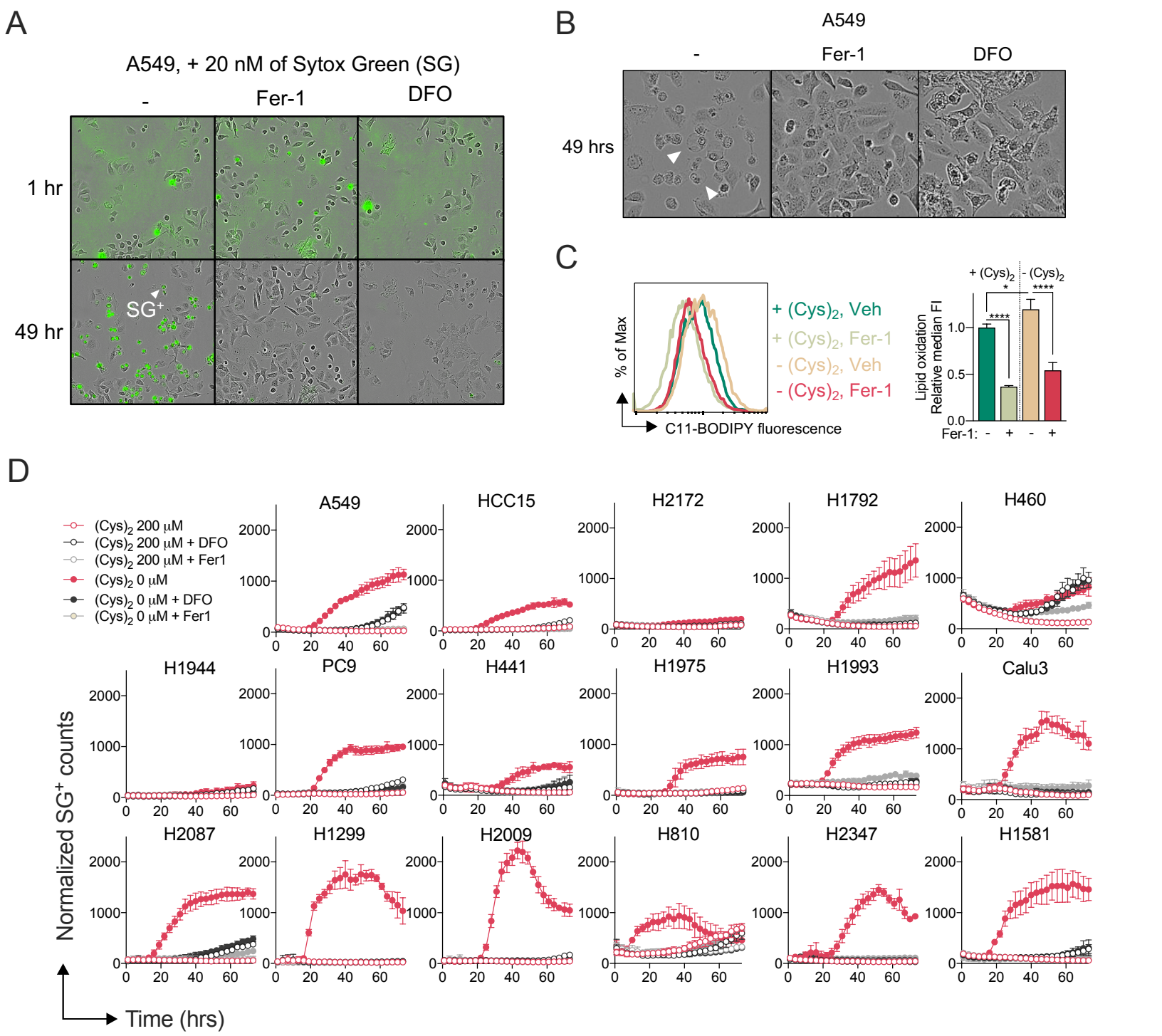
A
A549, + 20 nM of Sytox Green (SG)
-
Fer-1
DFO
1 hr
49 hr
SG+
B
A549
-
Fer-1
DFO
49 hrs
C
% of Max
C11-BODIPY fluorescence
+ (Cys)2, Veh
+ (Cys)2, Fer-1
- (Cys)2, Veh
- (Cys)2, Fer-1
Lipid oxidation
Relative median FI
+ (Cys)2
- (Cys)2
Fer-1: - + - +
D
(Cys)2 200 μM
(Cys)2 200 μM + DFO
(Cys)2 200 μM + Fer1
(Cys)2 0 μM
(Cys)2 0 μM + DFO
(Cys)2 0 μM + Fer1
A549
HCC15
H2172
H1792
H460
H1944
PC9
H441
H1975
H1993
Calu3
H2087
H1299
H2009
H810
H2347
H1581
Normalized SG+ counts
Time (hrs)

Figure S1. Transsulfuration cannot support NSCLC cysteine pools (related to Figure 1). (A) A representative image of Sytox Green (SG) stained A549 cells following cystine starvation for 1 or 49 hours in the presence of Vehicle (0.1% DMSO), Fer-1 (10 μM), or DFO (100 μM). Images show the same well position at the two different time points (1 or 49 hrs). A representative Sytox Green positive (SG^+) cell is indicated with a white arrow. (B) A representative image of non-stained A549 cells following 49 hours of cystine starvation treated with Vehicle (0.1% DMSO), Fer-1 (10 μM), or DFO (100 μM). Representative ferroptotic cells are indicated with white arrows. (C) Measurement of A549 cell lipid peroxidation under cystine starved (0 μM) or replete (200 μM) conditions treated with Vehicle (0.1% DMSO) or Fer-1 (10 μM) for 10 hrs (N=3). The median fluorescence intensity (median FI) of oxidized BODIPY-C11 signal was normalized by mean value of vehicle treated cystine replete conditions. (D) Incucyte time course measurement of NSCLC cell death under cystine starved (0 μM) or replete (200 μM) conditions treated with Vehicle (0.1% DMSO), Ferrostatin-1 (Fer-1, 10 μM) or DFO (100 μM) (N=4). Cell death was determined by Sytox Green every 3 hours over 73 hours and normalized to cell density. For C and D, data are shown as mean ± SD. N is the number of biological replicates. *P<0.05 and ****P<0.0001. For C, a one-way ANOVA with Bonferroni's multiple comparison test was used for statistical analyses.

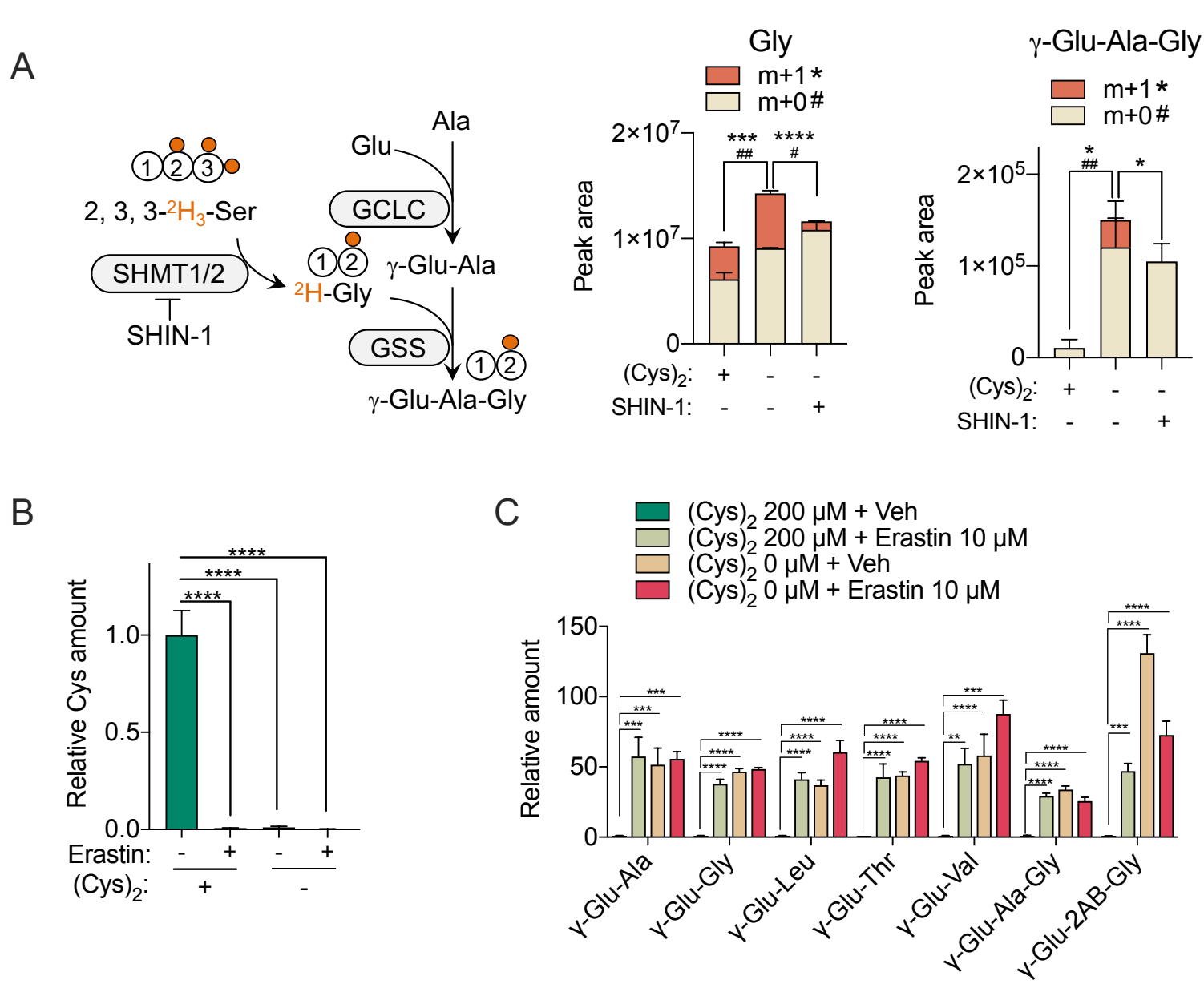
A
2, 3, 3-2H3-Ser
SHMT1/2
SHIN-1
2H-Gly
Glu
Ala
GCLC
γ-Glu-Ala
GSS
γ-Glu-Ala-Gly
Gly
m+1*
m+0#
Peak area
2×10^7
1×10^7
0
(Cys)2:
SHIN-1:
γ-Glu-Ala-Gly
2×10^5
1×10^5
B
Relative Cys amount
1.0
0.5
0.0
Erastin:
(Cys)2:
C
(Cys)2 200 μM + Veh
(Cys)2 200 μM + Erastin 10 μM
(Cys)2 0 μM + Veh
(Cys)2 0 μM + Erastin 10 μM
Relative amount
150
100
50
0
γ-Glu-Ala
γ-Glu-Gly
γ-Glu-Leu
γ-Glu-Thr
γ-Glu-Val
γ-Glu-Ala-Gly
γ-Glu-2AB-Gly

Figure S2. Cystine starvation induces glutamate-derived γ-glutamyl-peptide accumulation (related to Figure 2). (A) A549 cell 2, 3, 3-$^{2}H_{3}$-Ser tracing under cystine replete or starved conditions in the presence and absence of SHIN-1 (0.5 μM) for 12 hrs (N=3). (B-C) Intracellular (B) cysteine and (C) γ-Glu-peptides levels in A549 cells under cystine replete or starved conditions in the presence and absence of erastin (10 μM) for 12 hrs (N=3). For A-C, data are presented as mean ± SD. N is number of biological replicates. *P<0.05, **P<0.01, ***P<0.001, and ****P<0.0001; $^{\#}$P<0.05, $^{\#\#}$P<0.01. For A-C, a one-way ANOVA with Bonferroni's multiple comparison test was used for statistical analyses.

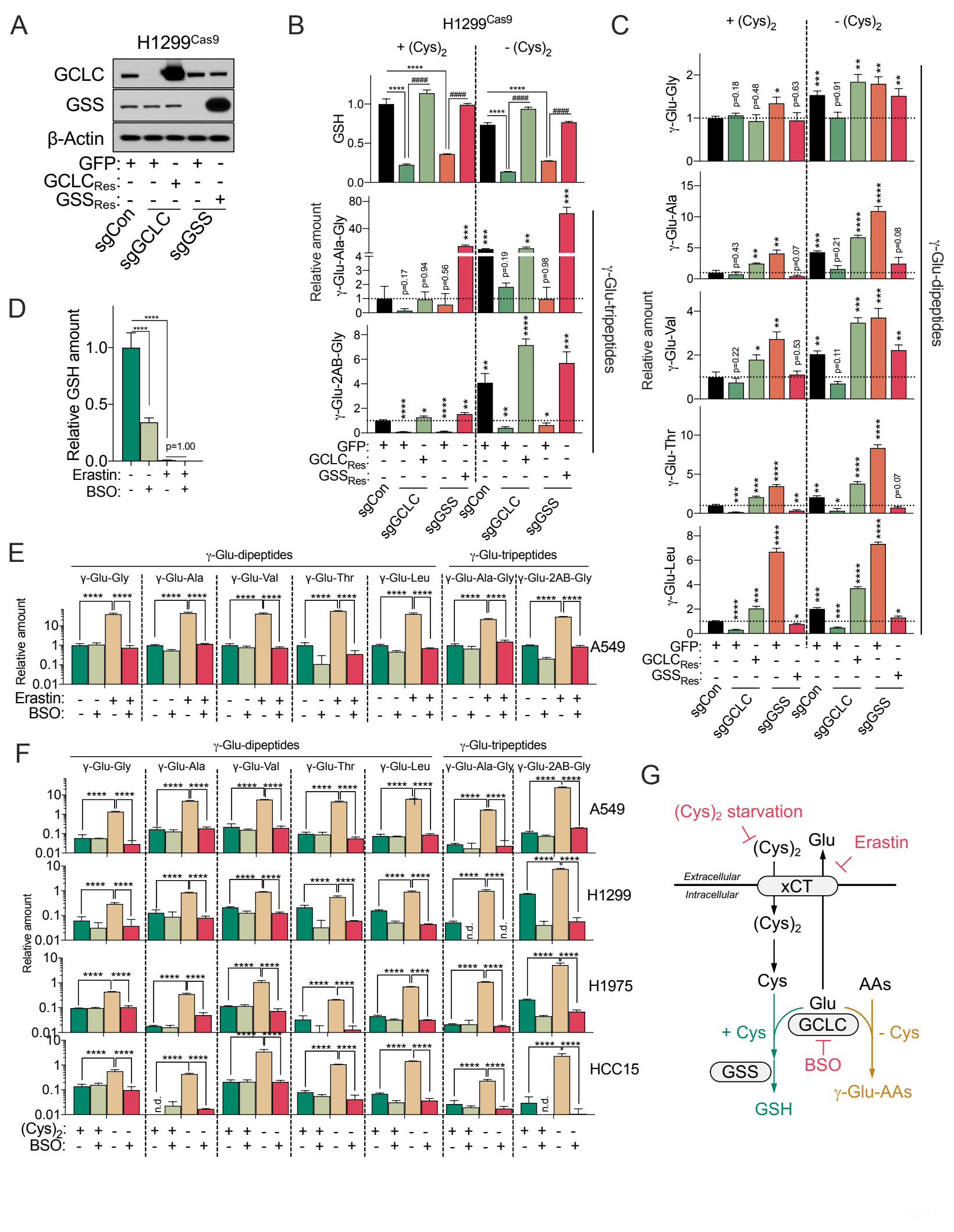
A
H1299Cas9
GCLC
GSS
β-Actin
GFP:
GCLCRes:
GSSRes:
sgCon
sgGCLC
sgGSS
B
H1299Cas9
+ (Cys)2
- (Cys)2
GSH
Relative amount
γ-Glu-Ala-Gly
γ-Glu-2AB-Gly
γ-Glu-tripeptides
C
γ-Glu-Gly
γ-Glu-Ala
γ-Glu-Val
γ-Glu-Thr
γ-Glu-Leu
γ-Glu-dipeptides
D
Relative GSH amount
p=1.00
Erastin:
BSO:
E
γ-Glu-dipeptides
γ-Glu-tripeptides
γ-Glu-Ala-Gly
γ-Glu-2AB-Gly
A549
F
H1299
H1975
HCC15
n.d.
(Cys)2:
G
(Cys)2 starvation
Glu
Erastin
Extracellular
Intracellular
xCT
Cys
AAs
+ Cys
- Cys
GCLC
BSO
GSS
GSH
γ-Glu-AAs

Figure S3. GCLC mediates γ-glutamyl-peptide synthesis in cell culture (related to Figure 3). (A) Representative immunoblots of GCLC and GSS expression from $H1299^{Cas9}$ cells transduced with sgRNAs (sgCon, sgGCLC or sgGSS), followed by reconstitution with GFP (+GFP), sgRNA-resistant GCLC (+$GCLC_{Res}$), or sgRNA-resistant GSS (+GSS_{Res}). β-actin was used as a loading control. (B-C) Intracellular γ-Glu-tripeptides (B) and γ-Glu-dipeptides (C) in the cells from (A) under cystine replete or starved conditions for 3 hrs (N=3). For B-C, data were normalized to the mean value of sgCon + GFP cells under cystine replete conditions. (D-E) Intracellular GSH (D) and γ-Glu-peptide levels (E) in A549 cells treated with erastin (10 μM) and/or BSO (100 μM) for 12 hrs (N=3). (F) Intracellular γ-Glu-peptides levels in four NSCLC cell lines under cystine replete or starved conditions in the presence and absence of BSO (100 μM) for 12 hrs (N=3). (G) Schematics depicting the effect of cystine availability and GCLC activity on γ-Glu-peptide production. For B - F, data are presented as mean ± SD. N is number of biological replicates. n.d. not detected. **P<0.01, ***P<0.001, and ****P<0.0001; ####P<0.0001. For GSH in B, one-way ANOVA with Bonferroni's multiple comparison test was used for the statistical comparison between sgCon + GFP, sgGCLC + GFP, and sgGSS + GFP. For the statistical comparison between sgGCLC + GFP and sgGCLC + $GCLC_{Res}$ or sgGSS + GFP and sgGSS + GSS_{Res}, an unpaired two-tailed t test was used. For γ-Glu-Ala-Gly and γ-Glu-2AB-Gly in B and C, an unpaired two-tailed t test was used for the comparison with parental cells under cystine replete conditions [+$(Cys)_2$]. For D-F, a one-way ANOVA with Bonferroni's multiple comparison test was used for statistical analyses.

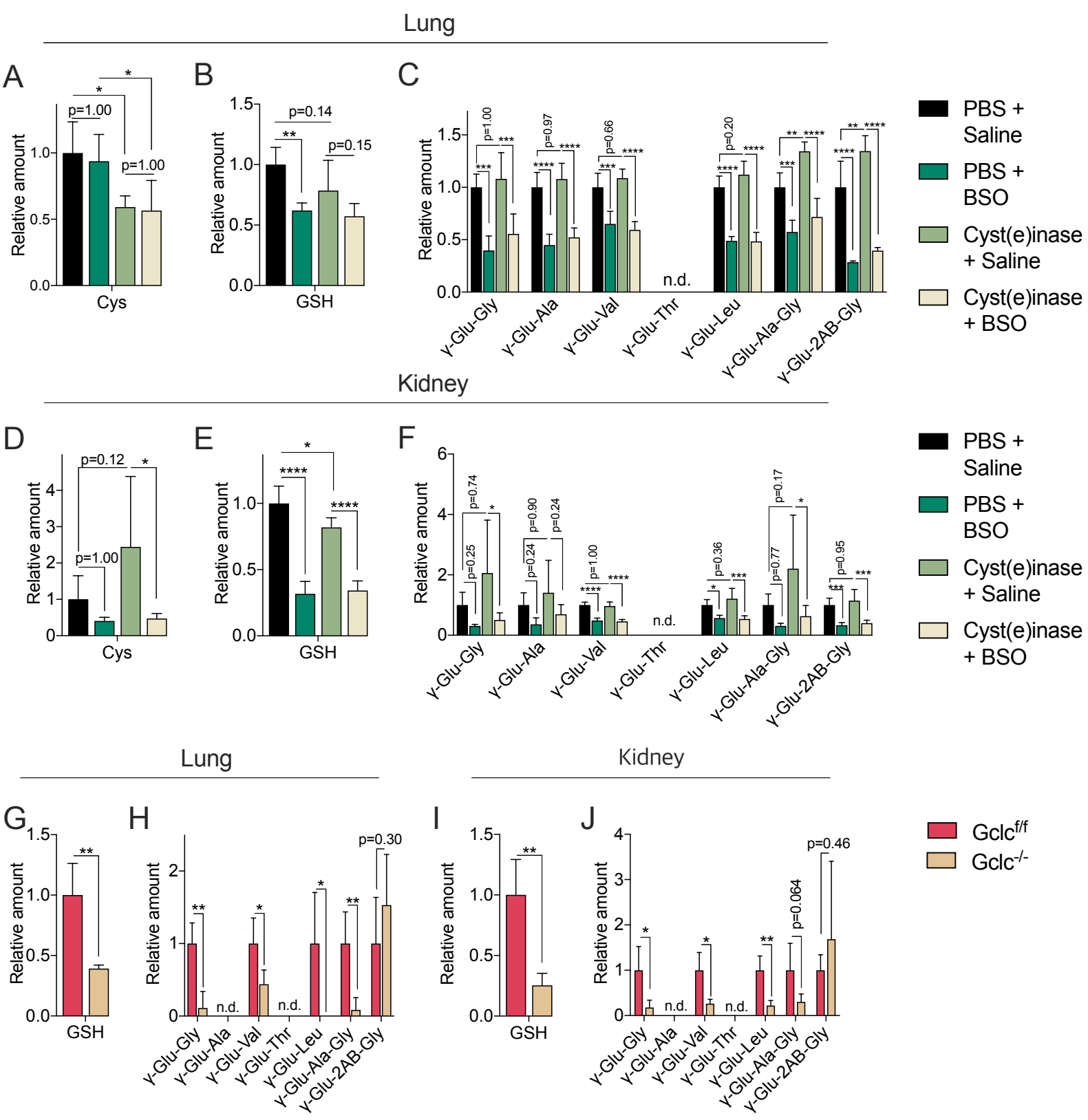
Lung
A
B
C
Relative amount
Cys
GSH
p=1.00
p=0.14
p=0.15
p=0.97
p=0.66
p=0.20
n.d.
γ-Glu-Gly
γ-Glu-Ala
γ-Glu-Val
γ-Glu-Thr
γ-Glu-Leu
γ-Glu-Ala-Gly
γ-Glu-2AB-Gly
PBS + Saline
PBS + BSO
Cyst(e)inase + Saline
Cyst(e)inase + BSO
Kidney
D
E
F
p=0.12
p=0.74
p=0.25
p=0.90
p=0.24
p=0.36
p=0.77
p=0.17
p=0.95
Lung
Kidney
G
H
I
J
Gclc^f/f
Gclc^-/-
p=0.30
p=0.46
p=0.064

Figure S4. GCLC mediates γ-glutamyl-peptide synthesis in vivo (related to Figure 4). (A-C) Analysis of lung cysteine (A), GSH (B), and γ-Glu-peptides levels (C) in mice treated with Cyst(e)inase or PBS, together with BSO or saline. (D-F) Analysis of kidney cysteine (D), GSH (E), and γ-Glu-peptides levels (F) in the mice from (A-C). The metabolite levels were normalized to the mean value of PBS/saline treated mice (N=5). (G-H) Analysis of lung GSH (G) and γ-Glu-peptides levels (H) in $Gclc^{f/f}$ and $Gclc^{-/-}$ mice. (I-J) Analysis of kidney GSH (I) and γ-Glu-peptides levels (J) in the mice from (G-H). The metabolite levels are normalized to the mean value of $Gclc^{f/f}$ mouse tissues (N=4). For A-J, data are presented as mean ± SD. N is number of biological replicates. n.d., not detected; *P<0.05, **P<0.01, ***P<0.001, and ****P<0.0001. For A-F, a one-way ANOVA with Bonferroni's multiple comparison test was used for statistical analyses. For G-J, an unpaired two-tailed t test was used for the statistical comparisons.

A

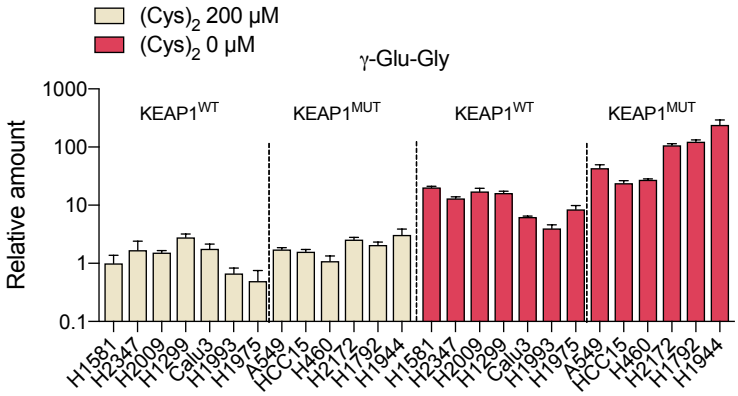
(Cys)2 200 μM
(Cys)2 0 μM
γ-Glu-Gly
Relative amount
KEAP1WT
KEAP1MUT
KEAP1WT
KEAP1MUT
1000
100
10
1
0.1
H1581 H2347 H2009 H1299 Calu3 H1993 H1975 A549 HCC15 H460 H2172 H1792 H1944

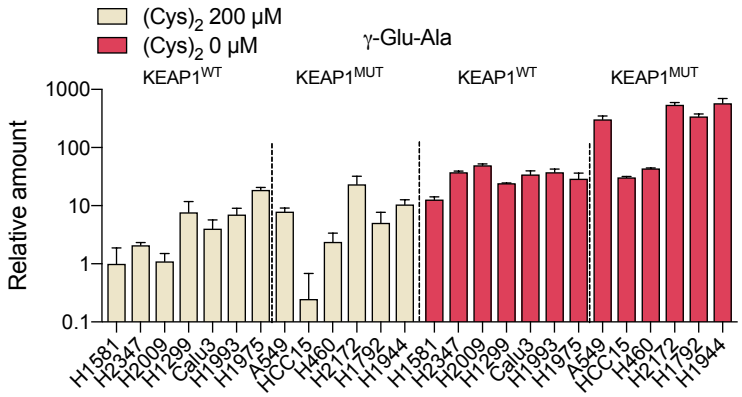
(Cys)2 200 μM
(Cys)2 0 μM
γ-Glu-Ala
Relative amount
KEAP1WT
KEAP1MUT
KEAP1WT
KEAP1MUT
1000
100
10
1
0.1
H1581 H2347 H2009 H1299 Calu3 H1993 H1975 A549 HCC15 H460 H2172 H1792 H1944

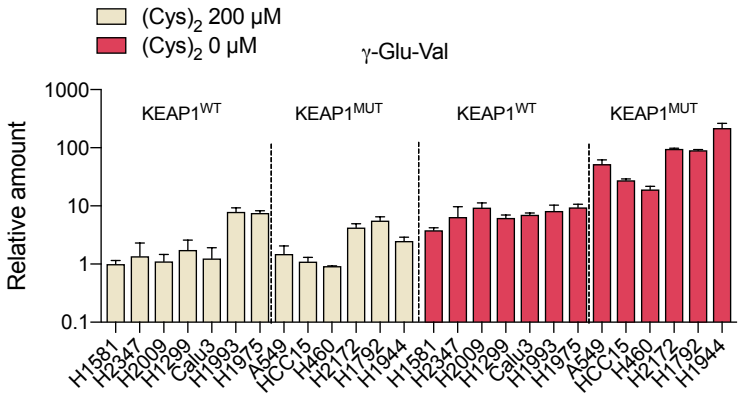
(Cys)2 200 μM
(Cys)2 0 μM
γ-Glu-Val
Relative amount
KEAP1WT
KEAP1MUT
KEAP1WT
KEAP1MUT
1000
100
10
1
0.1
H1581 H2347 H2009 H1299 Calu3 H1993 H1975 A549 HCC15 H460 H2172 H1792 H1944

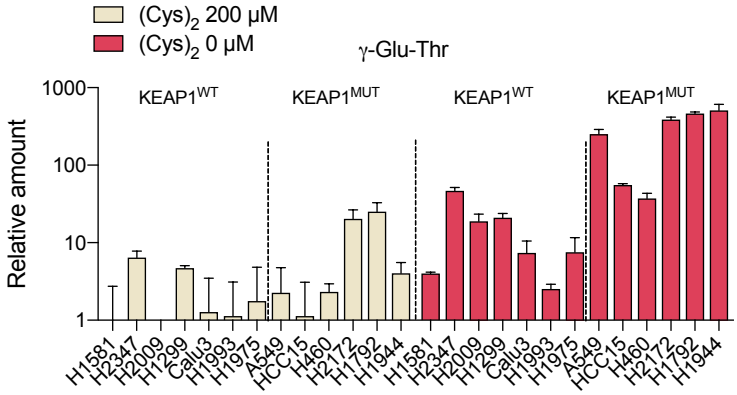
(Cys)2 200 μM
(Cys)2 0 μM
γ-Glu-Thr
Relative amount
KEAP1WT
KEAP1MUT
KEAP1WT
KEAP1MUT
1000
100
10
1
H1581 H2347 H2009 H1299 Calu3 H1993 H1975 A549 HCC15 H460 H2172 H1792 H1944

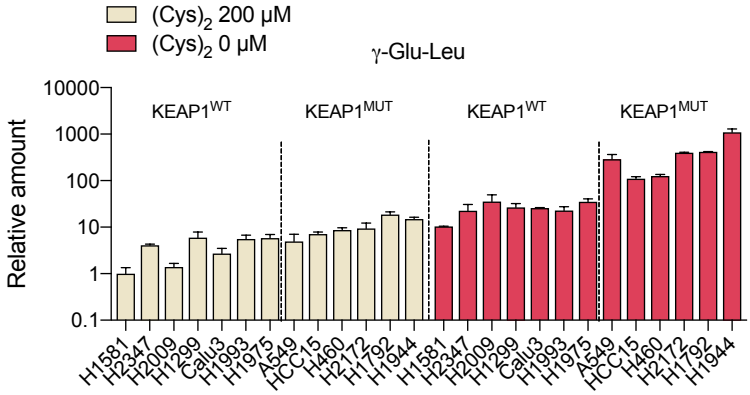
(Cys)2 200 μM
(Cys)2 0 μM
γ-Glu-Leu
Relative amount
KEAP1WT
KEAP1MUT
KEAP1WT
KEAP1MUT
10000
1000
100
10
1
0.1
H1581 H2347 H2009 H1299 Calu3 H1993 H1975 A549 HCC15 H460 H2172 H1792 H1944

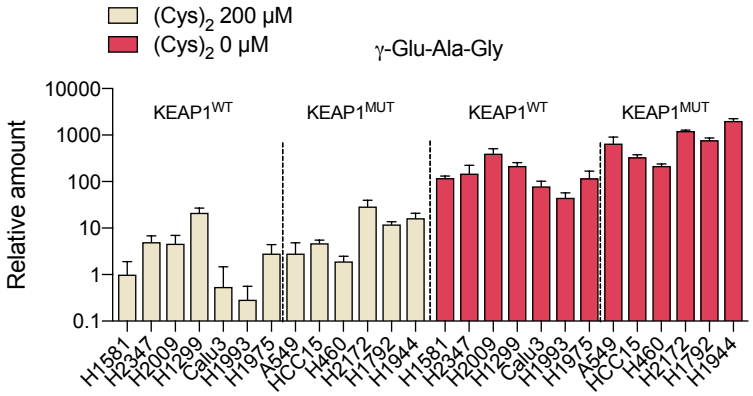
(Cys)2 200 μM
(Cys)2 0 μM
γ-Glu-Ala-Gly
Relative amount
KEAP1WT
KEAP1MUT
KEAP1WT
KEAP1MUT
10000
1000
100
10
1
0.1
H1581 H2347 H2009 H1299 Calu3 H1993 H1975 A549 HCC15 H460 H2172 H1792 H1944

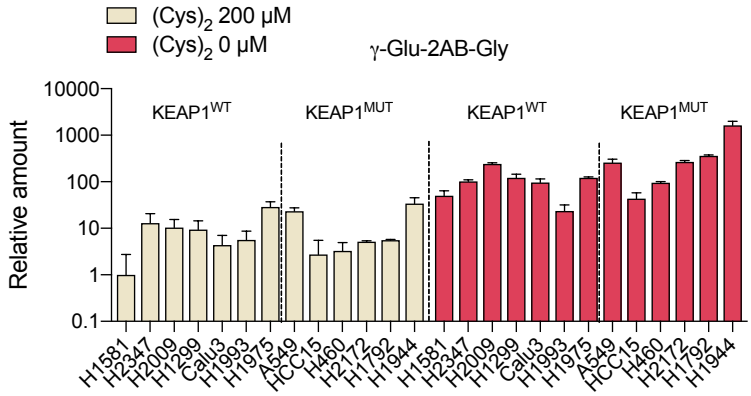
(Cys)2 200 μM
(Cys)2 0 μM
γ-Glu-2AB-Gly
Relative amount
KEAP1WT
KEAP1MUT
KEAP1WT
KEAP1MUT
10000
1000
100
10
1
0.1
H1581 H2347 H2009 H1299 Calu3 H1993 H1975 A549 HCC15 H460 H2172 H1792 H1944

Figure S5. NRF2 promotes γ-glutamyl-peptide synthesis via GCLC (related to Figure 5). (A) Analysis of relative γ-Glu-peptide levels in $KEAP1^{WT}$ (N=7) and $KEAP^{MUT}$ (N=6) NSCLC cell lines. The γ-Glu-peptides were analyzed following culture in cystine replete or starved conditions for 12 hrs. The γ-Glu-peptide amount of each NSCLC cell line was normalized to the mean value of H1581 cells under cystine replete conditions.

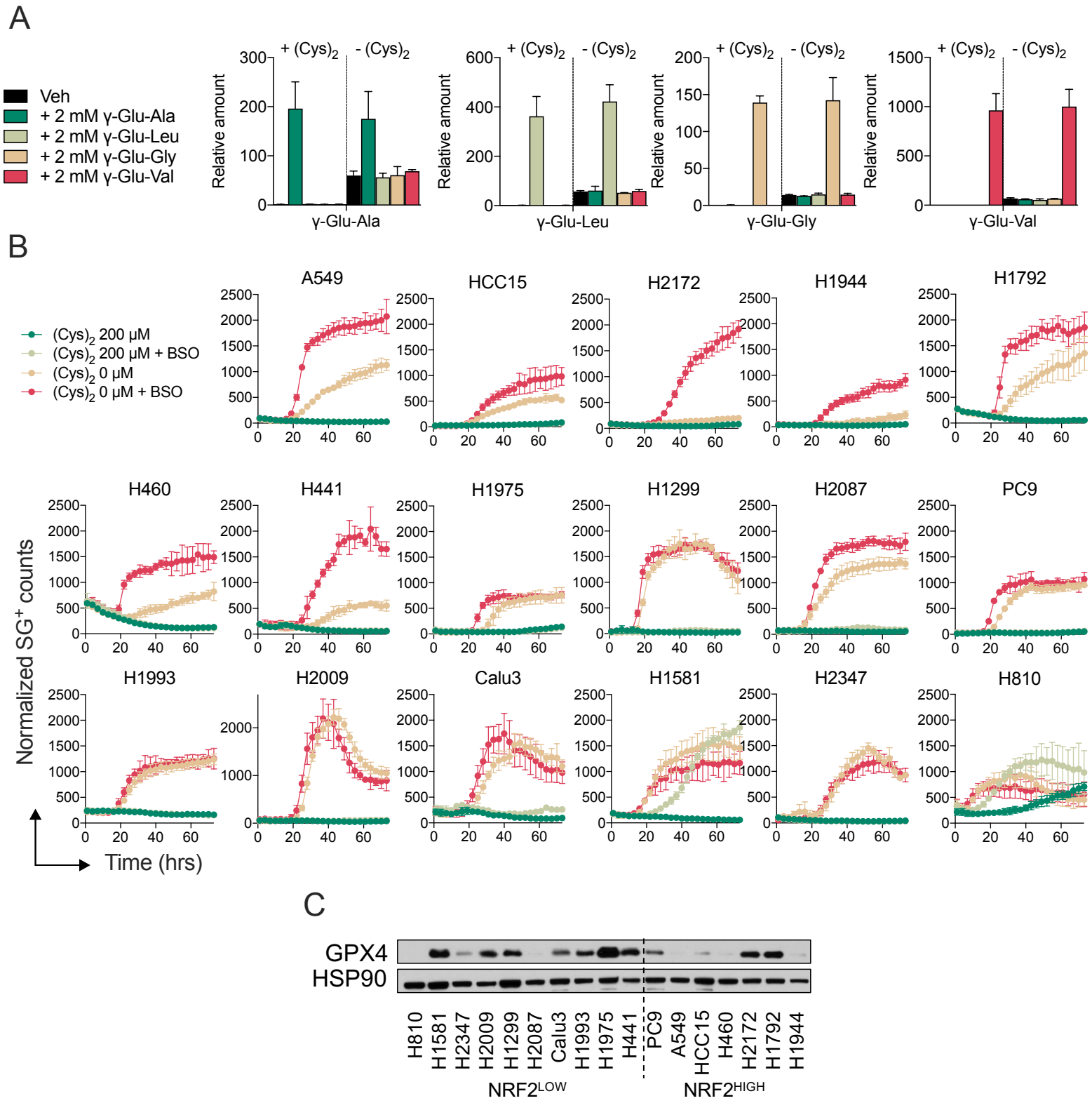
A
Veh
+ 2 mM γ-Glu-Ala
+ 2 mM γ-Glu-Leu
+ 2 mM γ-Glu-Gly
+ 2 mM γ-Glu-Val
+ (Cys)2
- (Cys)2
Relative amount
γ-Glu-Ala
γ-Glu-Leu
γ-Glu-Gly
γ-Glu-Val
B
(Cys)2 200 μM
(Cys)2 200 μM + BSO
(Cys)2 0 μM
(Cys)2 0 μM + BSO
A549
HCC15
H2172
H1944
H1792
H460
H441
H1975
H1299
H2087
PC9
H1993
H2009
Calu3
H1581
H2347
H810
Normalized SG+ counts
Time (hrs)
C
GPX4
HSP90
H810
H1581
H2347
H2009
H1299
H2087
Calu3
H1993
H1975
H441
PC9
A549
HCC15
H460
H2172
H1792
H1944
NRF2LOW
NRF2HIGH

Figure S6. Dipeptide synthesis protects KEAP1 mutant cells from ferroptosis (related to Figure 6). (A) Determination of the ability of exogenous γ-Glu-dipeptides to elevate intracellular γ-Glu-dipeptide levels. A549 cells were treated with the indicated concentration of γ-Glu-dipeptides for 12 hours under cystine replete and starved conditions and intracellular levels were assayed. γ-Glu-peptide amounts were normalized by the mean value of cystine replete conditions (N=3). (B) NSCLC cell death was monitored using Sytox Green (SG) every 3 hours with the Incucyte system. Cells were cultured under cystine starved or replete conditions and treated with vehicle (0.1% DMSO) or BSO (100 μM) for 73 hours (N=4). Vehicle-treated cystine replete and starved data are from Figure S1D. (C) Representative immunoblot of GPX4 expression in $NRF2^{LOW}$ and $NRF2^{HIGH}$ NSCLC cell lines. This blot is a reprobing of the GCLM blot shown in Figure 5A and shares the loading control (HSP90). For A and B, data are presented as mean ± SD. N is number of biological replicates.

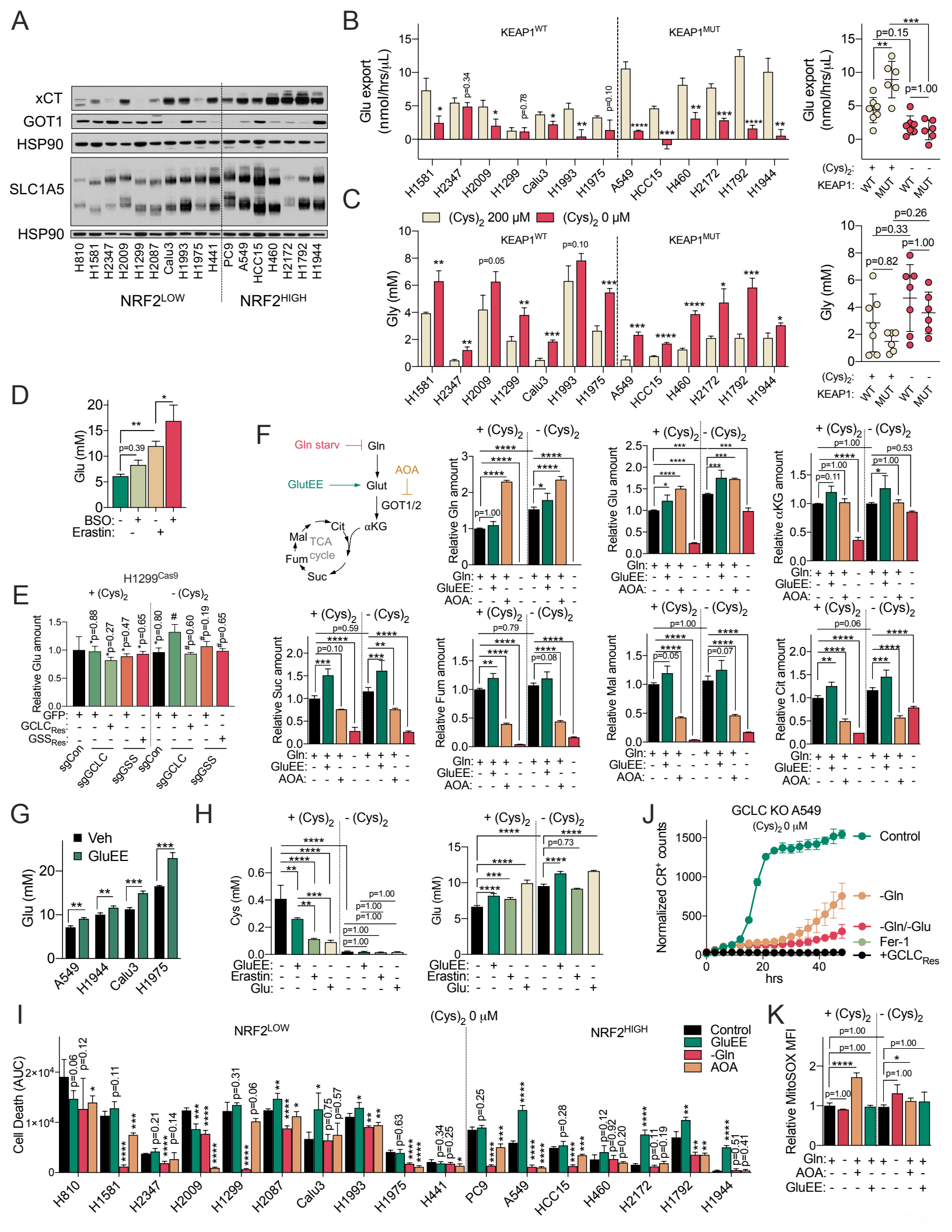
A
xCT
GOT1
HSP90
SLC1A5
HSP90
H810 H1581 H2347 H2009 H1299 H2087 Calu3 H1993 H1975 H441 PC9 A549 HCC15 H460 H2172 H1792 H1944
NRF2LOW
NRF2HIGH
B
KEAP1WT
KEAP1MUT
Glu export (nmol/hrs/μL)
H1581 H2347 H2009 H1299 Calu3 H1993 H1975 A549 HCC15 H460 H2172 H1792 H1944
p=0.15
p=1.00
(Cys)2: + + - -
KEAP1: WT MUT WT MUT
C
(Cys)2 200 μM
(Cys)2 0 μM
KEAP1WT
KEAP1MUT
Gly (mM)
p=0.26
p=0.33
p=1.00
p=0.82
D
Glu (mM)
p=0.39
BSO: - + - +
Erastin: - +
E
H1299Cas9
+ (Cys)2
- (Cys)2
Relative Glu amount
GFP:
GCLCRes:
GSSRes:
sgCon sgGCLC sgGSS sgCon sgGCLC sgGSS
F
Gln starv
Gln
GlutEE
Glut
AOA
GOT1/2
Cit
αKG
Mal
TCA cycle
Fum
Suc
Relative Gln amount
Relative Glu amount
Relative αKG amount
Relative Suc amount
Relative Fum amount
Relative Mal amount
Relative Cit amount
Gln:
GluEE:
AOA:
G
Veh
GluEE
Glu (mM)
A549 H1944 Calu3 H1975
H
Cys (mM)
Glu (mM)
GluEE:
Erastin:
Glu:
J
GCLC KO A549
(Cys)2 0 μM
Normalized CR+ counts
Control
-Gln
-Gln/-Glu
Fer-1
+GCLCRes
hrs
I
NRF2LOW
(Cys)2 0 μM
NRF2HIGH
Control
GluEE
-Gln
AOA
Cell Death (AUC)
H810 H1581 H2347 H2009 H1299 H2087 Calu3 H1993 H1975 H441 PC9 A549 HCC15 H460 H2172 H1792 H1944
K
+ (Cys)2
- (Cys)2
Relative MitoSOX MFI
Gln:
AOA:
GluEE:

Figure S7. Dipeptide synthesis scavenges glutamate (related to Figure 7). (A) Representative immunoblot of xCT, GOT1, and SLC1A5 in $NRF2^{LOW}$ and $NRF2^{HIGH}$ NSCLC cell lines. The xCT and GOT1 blots share a membrane with the NRF2 blot shown in Figure 5A and share the same loading control (HSP90). The SLC1A5 blot is a reprobing of the same membrane as the GCLC and GSS blots shown in Figure 5A and shares the loading control (HSP90). (B) (Left) Determination of the Glu export rate in NSCLC cell lines under cystine replete and starved conditions for 12 hrs (N=3). (Right) Comparison of the Glu export rate between KEAP1 ^{WT} (N=7) and KEAP1 ^{MUT} NSCLC (N=6) cells. (C) (Left) Analysis of intracellular Gly levels in NSCLC cell lines under cystine replete and starved conditions for 12 hrs (N=3). (Right) Comparison of Gly levels between KEAP1 ^{WT} (N=7) and KEAP1 ^{MUT} NSCLC (N=6) cells. (D) Analysis of intracellular Glu concentrations in A549 cells treated with erastin (10 μM) in the presence and absence of 100 μM BSO for 12 hrs (N=3). (E) Analysis of relative intracellular Glu levels in the $H1299^{Cas9}$ transduced with sgRNAs (sgCon, sgGCLC or sgGSS), followed by reconstitution with GFP (+GFP), sgRNA-resistant GCLC ($+GCLC_{Res}$), or sgRNA-resistant GSS ($+GSS_{Res}$) under cystine replete or starved conditions for 3 hrs (N=3). (F) Analysis of intracellular Gln, Glu, α-ketoglutarate (αKG), succinic acid (Suc), Fumaric acid (Fum), Malic acid (Mal), and Citric acid (Cit) under cystine replete and starved conditions for 12 hrs in the presence and absence of GluEE (5 mM), AOA (0.5 mM), or Gln starvation. (N=3). (G) Analysis of intracellular A549, H1944, Calu3, and H1975 cell Glu levels in the presence of GluEE (5 mM) for 12 hrs (N=3). (H) Analysis of intracellular A549 cell Cys (left) and Glu (right) levels following culture in cystine replete and starved conditions in the presence of GluEE (5 mM), Erastin (0.5 μM), or Glu (5 mM) for 12 hours (N=3). (I) Analysis of the death of NSCLC cell lines treated with GluEE (5 mM), AOA (0.5 mM) or starved of Gln. Cells were starved of cystine and cell death was monitored by Sytox Green every 3 hours for 49 hours, followed by AUC calculation. (N=4 except H1299, cystine 0 μM + GluEE: N=3). (J) Analysis of the death of GCLC KO A549 cells reconstituted with GCLC ($+GCLC_{Res}$), treated with Fer-1 (10 μM), or starved of Gln with or without Glu. Cells were starved of cystine for the indicated time points and death was monitored by Cytotox Red (CR) every 3 hours, and counts were normalized to density (N=3). (K) Analysis of A549 cell mitochondrial superoxide levels with MitoSOX under cystine starved and replete

conditions in the presence of AOA (0.5 mM), GluEE (5 mM), or Gln starvation for 8.5 hrs (N=3). MFI = mean fluorescence intensity. For B-K, data is presented as mean ± SD. N is number of biological replicates. *P<0.05, **P<0.01, ***P<0.001, and ****P<0.0001. For B (left), C (left), E, and G, unpaired two-tailed t tests were used for the statistical comparisons. For E, * is for the comparison with sgCon + GFP under cystine replete conditions [+$(Cys)_2$] and # is for the comparison between sg Con + GFP under cystine starved conditions [-$(Cys)_2$]. For B (right), C (right), D, F, H, I, and K, one-way ANOVA with Bonferroni's multiple comparison tests were used for statistical analyses.